The dual function monoclonal antibodies VIR-7831 and VIR-7832 demonstrate potent in vitro and in vivo activity against SARS-CoV-2

Andrea L. Cathcart[1], Colin Havenar-Daughton[1], Florian A. Lempp[1], Daphne Ma[1], Michael Schmid[2], Maria L. Agostini[1], Barbara Guarino[2], Julia Di iulio[1], Laura Rosen[1], Heather Tucker[1], Joshua Dillen[1], Sambhavi Subramanian[1], Barbara Sloan[1], Siro Bianchi[2], Jason Wojcechowskyj[1], Jiayi Zhou[1], Hannah Kaiser[1], Arthur Chase[1], Martin Montiel-Ruiz[1], Nadine Czudnochowski[1], Elisabetta Cameroni[1], Sarah Ledoux[1], Christophe Colas[1], Leah Soriaga[1], Amalio Telenti[1], Seungmin Hwang[1], Gyorgy Snell[1], Herbert W. Virgin[1], Davide Corti[2], Christy M. Hebner[1*]

[1]Vir Biotechnology, San Francisco, California 94158, USA

[2]Humabs Biomed SA, a subsidiary of Vir Biotechnology, 6500 Bellinzona, Switzerland

*corresponding author: chebner@vir.bio

ABSTRACT

VIR-7831 and VIR-7832 are dual action monoclonal antibodies (mAbs) targeting the spike glycoprotein of severe acute respiratory syndrome coronavirus 2 (SARS-CoV-2). VIR-7831 and VIR-7832 were derived from a parent antibody (S309) isolated from memory B cells of a 2003 severe acute respiratory syndrome coronavirus (SARS-CoV) survivor. Both mAbs contain an "LS" mutation in the Fc region to prolong serum half-life and potentially enhance distribution to the respiratory mucosa. In addition, VIR-7832 encodes an Fc GAALIE mutation that has been shown previously to evoke CD8+ T-cells in the context of an in vivo viral respiratory infection. VIR-7831 and VIR-7832 potently neutralize live wild-type SARS-CoV-2 in vitro as well as pseudotyped viruses encoding spike protein from the B.1.1.7, B.1.351 and P.1 variants. In addition, they retain activity against monoclonal antibody resistance mutations that confer reduced susceptibility to currently authorized mAbs. The VIR-7831/VIR-7832 epitope does not overlap with mutational sites in the current variants of concern and continues to be highly conserved among circulating sequences consistent with the high barrier to resistance observed in vitro. Furthermore, both mAbs can recruit effector mechanisms in vitro that may contribute to clinical efficacy via elimination of infected host cells. In vitro studies with these mAbs demonstrated no enhancement of infection. In a Syrian Golden hamster proof-of concept wildtype SARS-CoV-2 infection model, animals treated with VIR-7831 had less weight loss, and significantly decreased total viral load and infectious virus levels in the lung compared to a control mAb. Taken together, these data indicate that VIR-7831 and VIR-7832 are promising new agents in the fight against COVID-19.

INTRODUCTION

The coronavirus disease (COVID-19) pandemic caused by severe acute respiratory syndrome coronavirus 2 (SARS-CoV-2) has resulted in more than 114 million confirmed cases and over 2.5 million deaths

45 worldwide[1]. SARS-CoV-2 infection results in a broad range of disease severity[2]. Infection fatality rates
46 increase significantly with age, with 28.3% of COVID-19 patients over the age of 85 succumbing to
47 disease[2]. However, even in mild-to-moderate COVID-19 patients, significant post-infection sequelae can
48 affect overall health and cause long-term disability[3]. While multiple SARS-CoV-2 vaccines are now
49 authorized for use, issues of supply, vaccine hesitancy and emergence of variants may prevent rapid
50 attainment of herd immunity[4–9]. In addition, there may be individuals who remain at risk despite
51 vaccination due to disease or underlying immunodeficiency. Thus, additional interventions and potential
52 prophylactic agents are needed to reduce morbidity and mortality due to COVID-19.

53 Several monoclonal antibodies (mAbs) targeting the SARS-CoV-2 spike protein have recently been
54 authorized for use in early treatment of COVID-19 patients[10–13] and clinical data have been reported to
55 show promising results in treatment and prophylactic studies[12–15]. However, rapidly spreading variants
56 including those from the United Kingdom (B.1.1.7), South Africa (B.1.351) and Brazil (P.1) exhibit
57 reduced susceptibility in vitro to currently authorized antibodies that target the receptor binding motif
58 (RBM) of the viral spike (S) glycoprotein [10,11,16,17]. Therefore, mAbs targeting unique S epitopes are
59 needed for use alone or in combination with current agents for the treatment and prevention of COVID-
60 19. Furthermore, in addition to viral neutralization, antibodies possessing potent effector function to aid in
61 the killing of virally infected cells and the elicitation of T cell immunity could significantly assist in
62 halting disease progression[18–20].

63 VIR-7831 and VIR-7832 are dual action mAbs derived from the parent antibody S309 identified from a
64 2003 SARS-CoV survivor[21]. These mAbs target an epitope containing a glycan (at position N343) that is
65 highly conserved within the Sarbecovirus subgenus in a region of the S receptor binding domain (RBD)
66 that does not compete with angiotensin converting enzyme 2 (ACE2) binding[22]. This epitope does not
67 overlap with mutations observed in current variants of concern[10,11,16,17]. The variable region of VIR-7831
68 and VIR-7832 have been engineered for enhanced developability. In addition, both antibodies possess an
69 Fc "LS" mutation that confers extended half-life by binding to the neonatal Fc receptor and potentially

70 enhances distribution to the respiratory mucosa [23–25]. VIR-7832 is identical to VIR-7831 with the
71 exception of the addition of a 3 amino acid GAALIE (G236A, A330L, I332E) modification to the Fc
72 domain[26]. The GAALIE modification has previously been shown in vitro to enhance binding to FcγIIa
73 and FcγIIIa receptors, decrease affinity for FcγIIb compared to typical IgG1 and evoke protective CD8+
74 T-cells in the context of viral respiratory infection in vivo [27,28].

75 Here we characterize the antiviral potential of VIR-7831 and VIR-7832. These mAbs effectively
76 neutralize SARS-CoV-2 live virus in vitro as well as in pseudotyped virus assays against emerging
77 variants of concern and variants that confer resistance to currently authorized mAbs[29]. In addition to the
78 neutralizing capacity, both antibodies demonstrate potent effector function and mediate antibody
79 dependent cellular cytotoxicity (ADCC) and antibody dependent cellular phagocytosis (ADCP) in vitro.
80 Furthermore, resistance selection experiments and epitope conservation analyses indicate the potential for
81 a high barrier to resistance. Data derived from the Syrian golden hamster model demonstrates efficacy in
82 a proof-of-concept in vivo model. Taken together, these data indicate that VIR-7831 and VIR-7832 are
83 promising key components of the arsenal in the fight against COVID-19.

84 **RESULTS**

85 **VIR-7831 and VIR-7832 bind SARS-CoV-2 spike and effectively neutralize live virus in vitro.**
86 Previously published work showed that S309 bound SARS-CoV-2 recombinant and cell surface-
87 associated S and neutralized live virus in vitro[21]. We initiated these studies by repeating and extending
88 these earlier results. To determine the binding activity of VIR-7831 and VIR-7832 to the SARS-CoV-2 S,
89 enzyme-linked immunosorbent assay (ELISA), surface plasmon resonance (SPR) and flow cytometry
90 assays were utilized. VIR-7831 and VIR-7832 bound to recombinant S RBD (amino acids 331-541) with
91 EC_{50} values of 20.40 ng/mL and 14.9 ng/mL, respectively, by ELISA (**Figure 1a**). Using SPR, both
92 antibodies demonstrated potent binding to recombinant S RBD with an equilibrium constant (Kd) of 0.21
93 nM (**Figure 1b**). As antibody recognition of cell surface-bound S could mediate killing of virally infected
94 cells, flow cytometry-based studies using cells transiently transfected with a S-encoding plasmid were

95 used to examine antibody binding to cell surface-expressed S trimer. By this method, both VIR-7831 and
96 VIR-7832 bound efficiently to surface-expressed S (**Figure 1c**).

97 To examine neutralization capacity, VIR-7831 and VIR-7832 were tested in a VeroE6 cell-based live
98 SARS-CoV-2 virus system. Concentration-dependent viral neutralization was observed for both
99 antibodies, with geometric mean $IC_{50/90}$ values of 100.1/186.3 ng/mL and 78.3/253.1 ng/mL, respectively
100 (**Figure 1d**). As variant evolution is a natural part of SARS-CoV-2 biology and emerging live virus
101 variants are not always readily accessible for testing, a vesicular stomatitis virus (VSV)-based
102 pseudotyped virus system targeting Vero E6 cells was used to examine VIR-7831 and VIR-7832
103 neutralization of UK (B.1.1.7), South Africa (B.1.351) or Brazil (P.1) S. IC_{50} shifts were <1-fold for both
104 antibodies against the B.1.351 and P.1 pseudotyped viruses while small IC_{50} shifts were observed for the
105 UK pseudotyped virus (2.30- and 2.50-fold, respectively) indicating that VIR-7831 and VIR-7832 retain
106 activity against these spike variants (**Figure 1e; Table 1**). Interestingly, antibody neutralization of B.1.1.7
107 pseudotyped virus did not reach 100% in this assay though recently published data on the S309 mAb
108 against infectious B.1.1.7 showed that full neutralization was achieved[30].

109 **VIR-7831 and VIR-7831 exhibit potent effector function in vitro.** Although direct antiviral
110 mechanisms are crucial to provide protection, Fc-dependent mechanisms mediated by interaction with Fc
111 gamma receptors (FcγRs) on immune cells or with complement, can contribute to overall potency in vivo.
112 The potential for VIR-7831 and VIR-7832 to mediate effector functions were assessed in vitro by
113 measuring binding to FcγRs and C1q and in assays designed to demonstrate antibody-dependent cellular
114 cytotoxicity (ADCC) or antibody-dependent cellular phagocytosis (ADCP)[31–34].

115 Antibody binding to the human activating FcγRIIa (low-affinity R131 and high affinity H131 alleles),
116 FcγRIIIa (low-affinity F158 and high-affinity V158 alleles), and to the inhibitory FcγRIIb were examined
117 using SPR (**Supplemental figure 1a**). VIR-7831 similarly bound both the H131 and R131 alleles of
118 FcγRIIa and binds FcγRIIb. VIR-7831 bound both FcγRIIIa alleles, with reduced binding to the F158
119 allele compared to V158, as is characteristic for human IgG1[35]. Binding of VIR-7831 to C1q was similar

120 to the parental antibody (S309-LS) (**Supplemental figure 1b**). As previously reported for antibodies
121 encoding the GAALIE mutation[26,36], VIR-7832 bound with comparatively higher affinity to activating
122 FcγRIIa and FcγRIIIa than VIR-7831 (**Supplemental figure 1a**). Conversely, VIR-7832 showed reduced
123 affinity for FcγIIb and abrogation of binding to C1q (**Supplemental figure 1b**).

124 The antibodies were also assessed for the ability to activate human FcγRIIa, FcγRIIb or FcγRIIIa, using a
125 Jurkat cell reporter assay[37] (**Figure 2a-d**). S309-GRLR, which contains the effector function-abrogating
126 G236R, L328R mutations was used as a negative control. Cells stably transfected with the SARS-CoV-2
127 spike protein (CHO-CoV-2-Spike) served as target cells. Both VIR-7831 and the parental S309-LS
128 activated signaling of the higher-affinity allele FcγRIIa (H131) but did so less efficiently than the
129 GAALIE-containing antibody VIR-7832 (**Figure 1a**) while VIR-7831, VIR-7832 and S309-LS induced
130 similar low-level activation of the inhibitory receptor FcγRIIb (**Figure 1b**). VIR-7831 demonstrated
131 substantially lower activation of FcγRIIIa F158 versus V158 as expected while VIR-7832 showed
132 increased activation of both alleles of FcγRIIIa (F158 and V158) (**Figures c,d**).

133 To further elucidate the effector function potential of the antibodies, ADCC and ADCP assays were
134 performed using donor PBMCs or NK cells as effector cells and CHO cells stably expressing S (CHO-
135 CoV-2-Spike) as target cells (**Figure 2e-g**). The ability of antibodies to activate NK cell-mediated killing
136 was measured in vitro using two genotyped donors expressing homozygous low-affinity (F/F158) or high-
137 affinity (V/V158) (**Figure 2e-f**). Compared to the parental mAb S309-LS, VIR-7831 had slightly
138 increased capacity to induce NK cell-mediated ADCC when using cells from either F/F158 or V/V158
139 donors. As expected, VIR-7832 induced NK cell-mediated ADCC in cells from donors expressing the
140 low-affinity F/F158 allele of FcγIIIa more efficiently than VIR-7831. These results were confirmed with
141 NK cells from a heterozygous donor (F/V 158).

142 The ability of VIR-7831 and VIR-7832 to facilitate ADCP by primary $CD14^+$ monocytes was measured in
143 vitro by exposing freshly isolated human PBMCs to CHO-CoV-2-Spike cells that were pre-incubated
144 with antibody (**Figure 2g**). VIR-7831, VIR-7832 and S309-LS induced similar levels of ADCP by $CD14^+$

145 monocytes. These results indicate that VIR-7831 and VIR-7832 have the potential to trigger ADCC and
146 ADCP of cells displaying SARS CoV-2 S protein.

147 **Subneutralizing levels of VIR-7831 and VIR-7832 do not enhance virus uptake, replication or**
148 **cytokine production in vitro.** One potential concern with any antibody therapeutic targeting a viral agent
149 is the possibility of antibody-dependent enhancement (ADE). ADE is an in vivo phenomenon in which
150 the presence of an antibody worsens disease. There are several in vitro assays that may provide plausible
151 correlates for ADE in vivo, though none of these have been proven relevant to COVID-19 as to date ADE
152 has not been observed in trials of monoclonal antibodies or plasma[13,15,38,39]. ADE can occur by several
153 potential mechanisms[40]. Poorly neutralizing antibodies or subneutralizing levels of antibody could
154 theoretically facilitate enhanced virus entry and infection through Fc receptor interactions. A second
155 theoretical mechanism involves antibody-antigen complex formation leading to enhanced cytokine
156 production. A third mechanism of ADE has been observed in a porcine model of influenza where the
157 kinetics of viral fusion to the target cell was enhanced in a Fab-dependent manner by fusion-enhancing
158 non-neutralizing antibodies[41,42].

159 To explore whether VIR-7831 and VIR7832 exhibit in vitro activities that might be related to ADE in
160 vivo, we evaluated SARS-CoV-2 replication in human cells that express FcγRs: monocyte-derived
161 dendritic cells (moDCs), peripheral blood mononuclear cells (PBMCs) and the human U937 macrophage
162 cell line (**Supplemental Figure 2a-b**). Subneutralizing concentrations of VIR-7831 and VIR-7832 were
163 precomplexed with SARS-CoV-2 (MOI =0.01) and added to target cells. Using immunostaining methods,
164 at 24 hours post-infection no productive entry of SARS-CoV-2 into moDCs, PBMCs, or U937 cells was
165 observed in the presence or absence of either mAb, while VeroE6 control cells demonstrated
166 internalization in all conditions evaluated. Reduced internalization of SARS-CoV-2 in VeroE6 cells was
167 observed at the highest concentration of VIR-7831 and VIR-7832 (p-value <0.05), indicating effective
168 virus neutralization prevented virus entry. Using a focus forming assay, virus replication and secretion of
169 infectious virus were detectable by 48 hours post-infection in VeroE6 cells, with comparable levels of

170 replication in the presence or absence of VIR-7831 or VIR-7832. However, no replication of SARS-CoV-
171 2 was detected in moDCs, PBMCs or U937 cells regardless of antibody treatment, indicating lack of
172 productive SARS-CoV-2 infection of these cells, consistent with previously published data[43].

173 To evaluate the potential for VIR-7831 and VIR-7832 to enhance cytokine release upon SARS-CoV-2
174 infection in FcγR-expressing cells, cytokines and chemokines were measured in the supernatants from
175 cells infected with SARS-CoV-2-in the presence of VIR-7831 or VIR-7832 (**Supplemental figure 2c**).
176 Levels of IFN-γ, IL-10, IL-6, IL 8, IP-10, MCP-1, and TNF-α in the supernatant were quantified by MSD
177 at 24- and 48-hours post-infection. For all cell types evaluated, cytokine/chemokine production was
178 similar between all antibody concentrations tested and the no antibody control at both 24- and 48-hours
179 post-infection. Taken together, these in vitro data indicate that neither VIR-7831 nor VIR-7832 exhibit in
180 vitro activities that have been proposed to possibly correlate with ADE in vivo.

181 **VIR-7831 and VIR-7832 have a high barrier to resistance in vitro and do not display cross-**
182 **resistance with other SARS-CoV-2 mAbs.** We next determined whether resistant variants could be
183 elicited by serial passage of SARS-CoV-2 in the presence of VIR-7832. As VIR-7831 and VIR-7832
184 differ only in the Fc region of the antibody, resistance selection experiments were conducted with VIR-
185 7832 as a proxy for both antibodies. SARS-CoV-2 was subjected to 10 passages in the presence of VIR-
186 7832 at fixed concentrations of ~10x, 20x, 50x or 100x IC_{50} (1, 2, 5, or 10 μg/mL) in VeroE6 cells. No
187 CPE was detected in wells passaged with antibody through 10 passages, while CPE was observed in the
188 no antibody control in all passages. Similarly, no virus was detected by focus forming assay at any
189 concentration of VIR-7832 through all 10 passages even at the lowest concentration tested.

190 As no viral breakthrough was observed in the fixed concentration resistance selection, a second method
191 was employed wherein SARS-CoV-2 virus was passaged in sub-IC_{50} concentrations of antibody followed
192 by subsequent passaging in the presence of increasing concentrations of mAb in an attempt to force
193 resistance emergence (**Supplemental figure 3**). Passaging was performed in duplicate wells to account
194 for founder effects, and concentration increases for each well were based on CPE observations. Five

195 sequential passages were conducted using increasing concentrations of VIR-7832 at 0.5, 1, 2, 5 and ~10x
196 IC_{50} (0.05, 0.1, 0.2, 0.5, 1 µg/mL; **Supplemental figure 3a**), though no CPE was observed by passages 4
197 and 5 (0.5 and 1 µg/mL, respectively) indicating that variants originally selected at the lower
198 concentrations were either unfit or susceptible to the higher concentrations of antibody. To further assess
199 whether resistance mutations could be generated, selection was restarted using passage 3 virus generated
200 with ~2x IC_{50} (0.2 µg/mL) of VIR-7832 in duplicate wells at ~2x and ~5x IC_{50} (0.2, 0.5 µg/mL),
201 generating two passage lineages (**Supplemental figure 3b-c**).

202 Supernatants were evaluated for detectable virus at each passage by focus forming assay and cell
203 supernatants from viral passages containing detectable virus were tested in SARS-CoV-2 neutralization
204 assays to evaluate IC_{50} shifts as a marker of reduced susceptibility (**Supplemental table 1**). With the
205 exception of passage 8, modest fold changes were observed, with shifts in IC_{50} values ranging from 5.4-
206 to 6.5-fold compared to the wild-type SARS-CoV-2 stock virus. In lineage 1, the passage 8 virus
207 displayed a >10-fold shift in IC_{50} (greater than highest concentration tested). Sequence analysis detected
208 an identical 4 amino acid insertion in the N-terminal domain (215-216insKLRS) and 5 amino acid
209 deletion in correspondence of the furin cleavage site (675-679del) in both lineages at all passages
210 sequenced, as well as the amino acid substitution E340A in lineage 1, and R682W, and V1128F in
211 lineage 2. The deletion at amino acids 675-679 has been previously described during passaging of SARS-
212 CoV-2 in tissue culture suggesting enrichment to be a result of cell culture adaptation[44] while the 215-
213 216insKLRS was detected in the input virus. Neither 215-216insKLRS nor R682W variants were highly
214 enriched with passaging (**Supplemental Table 1**) and enrichment of 675-679del and V1128F did not
215 profoundly alter the VIR-7832 IC_{50}. However, appearance of the E340A variant at 98.7% did correlate
216 with a >10-fold shift in IC_{50} suggesting this variant may confer resistance.

217 To evaluate whether amino acid variants identified in the resistance selection conferred reduced
218 susceptibility to VIR-7831 and VIR-7832, neutralization of pseudotyped viruses encoding the S variants
219 was assessed (**Supplemental table 2**). VIR-7831 and VIR-7832 neutralized R682W and V1128F SARS-

220 CoV-2 pseudotyped virus spike variants with IC_{50} values similar to wild type (< 2-fold change in IC_{50})
221 indicating that these variants do not alter susceptibility. In contrast, E340A conferred reduced
222 susceptibility to VIR-7831 and VIR-7832 (> 100-fold change in IC_{50}) indicating that E340A is a VIR-
223 7831/VIR-7832 monoclonal antibody resistance mutation (MARM).

224 As VIR-7831/VIR-7832 demonstrated a unique in vitro resistance profile, we investigated the potential
225 for cross-resistance to MARMs that confer reduced susceptibility to the authorized monoclonal antibodies
226 bamlanivimab, imdevimab and casirivimab [10,11,45–47] using pseudotyped virus. Notably, some of these
227 mutations are found in highly prevalent variants of concern[17,30,48]. VIR-7831 effectively neutralized
228 pseudotyped viruses expressing spike MARMs that alter bamlanivimab, casirivimab and/or imdevimab
229 activity (**Table 2**). Fold changes in IC_{50} values compared to wild-type were <3-fold for 18/19 variants
230 tested. A modest 3.4-fold shift in the VIR-7831 IC_{50} was observed for the V445A variant that confers
231 reduced susceptibility to imdevimab. These data indicate that VIR-7831/VIR-7832 does not display cross-
232 resistance with currently authorized mAbs and supports the potential combination use of VIR-7831/VIR-
233 7832 with other mAb therapeutics.

234 **The VIR-7831/VIR-7832 epitope is highly conserved among SARS-CoV-2 sequences.** The parental
235 antibody of VIR-7831 and VIR-7832 (S309) binds to a highly conserved sarbecovirus epitope that is
236 potentially intolerant of variation. To investigate the current state of epitope conservation, >584,000 spike
237 sequences from SARS-CoV-2 deposited in the GISAID database as of February 26, 2021 were examined
238 for epitope variation. More than 99.96% conservation is seen for those amino acids comprising the
239 epitope among currently available sequences for all positions including 14/22 amino acid positions that
240 were ≥99.99 conserved (**Table 3**).

241 VIR-7831 activity against viral mutants carrying single substitutions in the epitope was assessed in
242 pseudotyped virus assays. VIR-7831 effectively neutralized epitope variants at most amino acid positions
243 tested (**Table 4**). Variants at two positions, E340 and P337, resulted in significant IC_{50} shifts indicating
244 reduced susceptibility to VIR-7831. Moderate shifts in potency were observed for P337H and P337T

245 variants (7.50- and 5.38-fold, respective) while more significant shifts in potency were observed for
246 P337L/R and E340A/K/G (27-fold to >276-fold). Notably, these variants are detected in a low number of
247 sequences and do not have a pattern that suggest emergence in the GISAID database (27 and 30 variant
248 counts out of >584,000 sequences for P337 and E340, respectively). This observation is consistent with
249 the possibility that variations at these positions come with a fitness cost to the virus.

250 **VIR-7831 reduces weight loss, total viral load and infectious virus levels in a hamster model of**
251 **SARS-CoV-2 infection.** To evaluate the efficacy of VIR-7831 in vivo, the hamster model was utilized.
252 As it was unknown what effect the LS mutation would have in the hamster, a non-LS version of VIR-
253 7831 (SGHmAb-no-LS) was used for these experiments. Hamsters were administered SGHmAb-no-LS
254 intraperitoneally at Day -1 (30, 5, 0.5 or 0.05 mg/kg) or Day -2 (15, 5, 0.5 or 0.05 mg/kg) prior to
255 intranasal SARS-CoV-2 inoculation (**Figure 3a**). Satellite animal PK indicated that maximal antibody
256 serum concentrations were achieved at Day 2 and Day 1 for Day -1 and Day -2 dosing, respectively.
257 Using body weight as a marker of degree of clinical disease, doses of ≥5mg/kg resulted in significantly
258 reduced weight loss at Day 4 compared to controls. (**Figure 3b-e**). Significant decreases in lung viral load
259 were also observed at ≥5mg/kg as measured by RT-qPCR (**Figures f-g**). Day 4 $TCID_{50}$ measurements
260 indicated that antibody administered at ≥0.5 mg/kg resulted in significantly lower levels of infectious
261 virus in lung tissue compared to controls (**Figure 3h-i**). Notably, across these experiments, no
262 enhancement of disease was observed in animals receiving SGHmAb-no-LS based on changes in weight,
263 viral RNA in the lungs, or $TCID_{50}$ infectious virus levels. Collectively, these data indicate that VIR-7831
264 prevented in a dose-dependent fashion virus replication and morbidity in SARS-CoV-2 challenged
265 hamsters without signs of ADE at any dose tested.

266 **DISCUSSION**

267 Here we show the in vitro and in vivo preclinical characterization of VIR-7831 and VIR-7832, two
268 monoclonal antibodies being advanced into clinical studies[49–51]. Both antibodies demonstrate high-affinity
269 binding to S in vitro, including on the surface of cells, and effectively neutralize wildtype SARS-CoV-2

270 in a live virus assay. VIR-7831 and VIR-7832 retain activity against the UK B.1.1.7, South Africa
271 B.1.351 and Brazil P.1 variants in a VSV/VeroE6 pseudotyped virus system, consistent with recently
272 published data using live viruses [29]. VIR-7831 bind C1q, activate FcγRs and demonstrate ADCC and
273 ADCP in vitro. Experiments in the hamster model of SARS-CoV-2 infection show proof-of-concept
274 efficacy in vivo. Notably, in vitro and in vivo data did not provide any supporting evidence that these
275 antibodies would demonstrate ADE in a clinical setting.

276 That VIR-7831 and VIR-7832 retain activity against the B.1.1.7, B.1.351 and P.1 spike proteins in
277 pseudotyped virus assays is a key finding at this stage of the pandemic. With the increased
278 transmissibility and potential for more severe disease observed with these viruses, the availability of
279 therapeutic or prophylactic mAbs that remains active against these variants is essential. Current in vitro
280 data indicate that the E484K variant found in both B.1.351, P.1 and other emerging independent lineages,
281 and also recently found in combination with B.1.1.7[52], confers reduced susceptibility to multiple currently
282 authorized monoclonal antibodies possibly lessening the utility of these antibodies or, worse, rendering
283 them ineffective. In addition to retaining activity against key variants of concern, in pseudotyped virus
284 experiments VIR-7831 showed no significant cross-resistance with variants that reduce the activity of
285 authorized mAbs. These data additionally demonstrate the uniqueness of VIR-7831 and VIR-7832 and
286 further highlight the utility VIR-7831 and VIR-7832 could have, alone or in combination, as clinical
287 agents.

288 Notably, even over a year into the pandemic, the VIR-7831/VIR-7832 epitope remains highly conserved
289 among available sequences of circulating virus with ≥99.96% conservation of epitope amino acids. This is
290 consistent with the value of the strategy used for isolation of monoclonal antibodies that neutralize both
291 SARS-CoV and SARS-CoV-2 based on the idea that these two virulent human viruses are
292 phylogenetically divergent within the sarbecovirus subgenus. Furthermore, MARMs identified at
293 positions P337 and E340 are present at very low levels among current sequences. That amino acids P337
294 and E340 remain >99.99% conserved at this stage of the pandemic indicates that variants at these

295 positions may confer disadvantageous effects on the virus, consistent with the conservation of this epitope
296 across the sarbecovirus family[21].

297 Viral variants of concern for RBM-targeting mAbs are already spreading[53]. The vaccines presently being
298 deployed around the world generate high-titer neutralizing antibodies that target the S protein RBM.
299 Importantly, the RBM is highly immunodominant for responses to natural infection[54]. Vaccine-induced
300 and convalescent immunity may therefore potentially put further mutational pressure on the RBM
301 sequence to evade such antibody responses. In contrast, antibody responses overlapping with the VIR-
302 7831/VIR-7832 epitope are limited after infection [54], possibly because of the shielding effect of the highly
303 conserved N343 glycan. In this regard the epitope may face less vaccine- or infection-generated immune
304 pressure, potentially preserving this conserved epitope long-term.

305 Recent data have indicated that the cells used to generate live virus stocks and overexpression of
306 ACE2/TMPRSS2 in target cells used for assays can affect mAb activity in vitro[29,55]. The VIR-7831/VIR-
307 7832 parental antibody S309 seems particularly sensitive to in vitro methods using ACE2 overexpressing
308 cells[55]. It is therefore notable that VIR-7831 displays significant efficacy in an in vivo proof-of-concept
309 SARS-CoV-2 infection experiment using hamsters despite the fact that patterns of engagement of hamster
310 FcRs by human IgG1 antibodies may not reflect patterns of human IgG1 antibodies with their cognate
311 human FcRs. These findings argue that in vitro data derived from such ACE2 and/or TMPRSS2
312 overexpression cell lines do not accurately reflect the in vivo antiviral capacity of tested mAbs.
313 Furthermore, that the significant in vivo effects of VIR-7831 in the hamster model likely occurred in the
314 absence of full effector functions due to species-specific interactions between antibodies and FcRs, argues
315 that effects in COVID-19 patients incorporating both the neutralization capacity of the antibody plus the
316 ability to harness the strength of the immune system could lead to positive clinical outcomes.

317 The clinical potential of VIR-7832, with the inclusion of the GAALIE Fc mutation, is of special interest
318 in the context of SARS-CoV-2 infection. Previously published data by the Ravetch laboratory comparing
319 the in vivo efficacy of a hemagglutinin-targeting mAb with and without inclusion of the GAALIE

320 mutation in a transgenic humanized FcγR mouse model of influenza infection demonstrated superior
321 efficacy of the GAALIE-containing antibody in both therapeutic and prophylactic experiments[26]. These
322 effects were mediated by protective $CD8^+$ T cell responses elicited by the GAALIE antibody. Clinical
323 data examining the contribution of the adaptive immune response in SARS-CoV-2 infection indicate that
324 poor T cell induction correlates with severe disease (reviewed in [56]). Thus, the potential for VIR-7832 to
325 augment the T cell response to SARS-CoV-2 infection could conceivably play a crucial role in limiting
326 progression to severe COVID-19 disease or in treatment of severe established disease. This latter
327 possibility is supported by recent publications showing that monoclonal antibodies with effector functions
328 are especially effective in the therapeutic setting via recruitment of tissue-protective monocyte functions
329 [19], and that potency of antibodies in the pre-clinical mouse model does not correlate with in vitro
330 neutralizing activity of antibodies[18].

331 Taken together, these data indicate that VIR-7831 and VIR-7832 could play a powerful role in the fight
332 against COVID-19 through the dual action of broadly neutralizing activity paired with engagement of the
333 immune system through effector function capabilities.

334

335 **METHODS**

336 **Cells.** Vero E6 cells (ATCC) and Lenti-X 293T cells (Takara) were cultured in Dulbecco's Modified
337 Eagle's medium (DMEM), 10% FBS, 1x Penicillin-Streptomycin at 37°C, 5% CO_2.

338 **Monoclonal Antibodies.** VIR-7831 and VIR-7832 were produced at WuXi Biologics (China). SGHmAb-
339 no-LS, S309-LS, and S309-GRLR were produced at Humabs Biomed SA, a subsidiary of Vir
340 Biotechnology (Bellinzona, Switzerland) in expiCHO cells transiently co-transfected with plasmids
341 expressing the heavy and light chain, as previously described [57].

342 **Virus. S**ARS-CoV-2 isolate USA-WA1/2020 was obtained from BEI Resources. Virus was propagated
343 on VeroE6 cells in DMEM, 2% BSA, 1X Penicillin-Streptomycin at 37°C, 5% CO_2. Supernatants were

344 collected at 72 hours post-infection once cytopathic effect was visible, centrifuged at 500 x g for 5
345 minutes, followed by a second centrifugation at 1000 x g for 5 minutes. Clarified supernatants were then
346 aliquoted and stored at -80°C.

347 **In vitro binding ELISA.** For the ELISA assay, 96-well plates were coated with 100 µl/well recombinant
348 SARS-CoV2 RBD diluted in assay diluent (1% BSA/PBS) at a final concentration of 2 µg/mL and
349 incubated overnight at 4°C. Plates were washed three times with 300 µl/well wash buffer using an
350 automated washer. Assay diluent (100 µl/well) was added to block the plates and incubated for 1 hour at
351 room temperature (RT) with shaking. Assay diluent was removed, and plates washed three times with
352 wash buffer. Serial 1:3 dilutions of mAb (concentration range from 6 µg/mL to 0.33 ng/mL) in assay
353 diluent were dispensed at 100 µl/well and incubated 1 hour at RT with shaking, then washed three times
354 with wash buffer. The HRP-conjugated secondary antibody reagent (1:5,000 dilution in assay diluent)
355 was added to each well (100 µl/well) and incubated for 1 hour at RT with shaking. After three washes
356 with wash buffer, 100 µl/well of 2-component TMB peroxidase substrate solution was dispensed in each
357 well and developed for 5 minutes at RT. The reaction was stopped with 100 µL/well 1M H_2SO_4 and the
358 OD was read immediately at 450 nm on a SpectraMax M5 Microplate reader. EC_{50} values were calculated
359 using non-linear regression of log (agonist) versus response in Graph Pad Prism.

360 **Spike binding affinity quantification by SPR.** Antibody was diluted to 2 µg/mL (1 mL) in HBS-EP+
361 buffer and injected at 10 µL/min for 30 seconds across one flow cell of a CM5 sensor chip immobilized
362 with anti-human Fc antibody docked in a Biacore T200. SARS-CoV2-RBD diluted in HBS-EP+ buffer
363 was then injected at a single concentration, 1:3 dilutions from 100 nM to 3.7 nM, across both the flow cell
364 containing captured the antibody as well as a reference flow cell containing only anti-human Fc antibody.
365 Binding was measured with a flow rate of 30 µL/min and an injection time of 600 seconds; dissociation
366 was monitored for 1800 seconds after injection. Data were collected at 10 Hz. After each binding
367 measurement, regeneration reagent was injected to prepare the surface for a new cycle. Experiments were
368 performed at 25°C, with the samples held at 15 °C in the instrument prior to injection.

369 **Measurement of Binding to Human Fcγ Receptors by SPR.** Binding of VIR-7831 and VIR-7832 to
370 human recombinant FcγRs was measured by surface plasmon resonance (SPR) on a Biacore T200.
371 Briefly, Biotin CAPture Reagent (modified streptavidin) was injected across all flow cells of a CAP
372 sensor chip docked in a Biacore T200. Biotinylated Fc receptors at 1 µg/mL were injected across a single
373 flow cell at 10 µL/min for 60 seconds (one receptor per flow cell), with one flow cell reserved as a
374 reference surface. VIR 7831 or VIR-7832 at 100 µg/mL (diluted in HBS-EP+) were injected across all
375 flow cells for 200 seconds using a flow rate of 30 µL/min and association was monitored. Dissociation
376 was monitored for another 200 seconds after injection. Data was collected at 10 Hz. After each binding
377 measurement, CAP Regeneration reagent was injected to prepare the surface for a new cycle.
378 Experiments were performed at 25°C, with the samples held at 15°C in the instrument prior to injection.

379 **Measurement of Binding to Human Complement Protein C1q.** Binding of VIR-7831 and VIR-7832 to
380 human complement was measured by biolayer interferometry (BLI) using an Octet Red96 instrument
381 (FortéBio). Briefly, anti-human Fab (CH1-specific) sensors were used to capture VIR-7831 and VIR-
382 7832 at 10 µg/ml for 10 minutes. The IgG-loaded sensors were then exposed to kinetics buffer containing
383 3 µg/ml of purified human C1q for 4 minutes, followed by a dissociation step in the same buffer for
384 additional 4 minutes. Association and dissociation profiles were measured in real time as changes in the
385 interference pattern.

386 **Binding to Cell Surface Expressed SARS-CoV-2 Spike Protein.** The SARS-CoV-2 spike protein
387 coding sequence (YP_009724390.1, Wuhan-Hu-1 strain) was cloned into a cell expression plasmid under
388 the control of the human CMV promoter (phCMV1) to generate phCMV1 WT spike. ExpiCHO-S cells
389 were seeded the day before transfection at 3 x 10^6 cells/mL in ExpiCHO Expression Medium.
390 Immediately before transfection, the cells were seeded at 6 x 10^6 cells cells/mL in a volume of 15 mL in
391 125 mL shake flasks. Six µg of phCMV1 WT spike plasmid or vector control were diluted in 1.2 mL of
392 iced OptiPRO SFM., followed by addition of 48 µL of ExpiFectamine CHO Reagent and complexing for
393 1 minute at RT. The transfection mixture was added dropwise to cells with gentle swirling. Cells were

394 then incubated at 37°C, 8% CO2 with shaking for 42 hours. At 42 hours post-transfection, ExpiCHO-S
395 cells were harvested, washed twice with FACS buffer and resuspended at a concentration of 1.0 x 10^6
396 cell/mL in PBS. Cells (5 x 10^4 cells in 50 µl/wells) were dispensed into a 96-well V-bottom plate.
397 Antibody was serially diluted (1:4, 10 points) starting at a concentration of 10 µg/mL. Cells were pelleted
398 at 300 x g for 5 minutes and resuspended in 50 µL/well of antibody serial dilutions and plates were
399 incubated for 45 mins on ice. Cells were washed twice in FACS buffer. Alexa Fluor 647-labelled Goat
400 Anti-Human IgG secondary Ab was diluted 1:750 in FACS buffer and 50 µL was added to the cell pellet
401 for 15 min on ice. Cells were washed twice with FACS buffer, resuspended in 1% PFA. Data was
402 acquired by flow cytometry (CytoFlex LX).

403 **Pseudotyped virus production.** Lenti-X™ 293T cells were seeded in 10-cm dishes for 80% next day
404 confluency. The next day, cells were transfected with the plasmid pcDNA3.1(+)-spike-D19 (encoding the
405 SARS-CoV-2 spike protein) or pcDNA3.1(+)-spike-D19 variants using the transfection reagent TransIT-
406 Lenti according to the manufacturer's instructions. One day post-transfection, cells were infected with
407 VSV-luc (rVSVΔG; Kerafast) at an MOI of 3. The cell supernatant containing SARS-CoV-2 pseudotyped
408 virus was collected at day 2 post-transfection, centrifuged at 1000 x g for 5 minutes to remove cellular
409 debris, aliquoted and frozen at -80°C.

410 **In Vitro Neutralization of SARS-CoV-2 Pseudotyped Virus.** Vero E6 cells were seeded into clear
411 bottom black walled 96-well plates at 20,000 cells/well in 100 µL medium and cultured overnight at
412 37°C. Twenty-four hours later, 1:4 9-point serial dilutions of antibody were prepared in media, with each
413 dilution tested in duplicate on each plate (range: 10 µg/mL to 0.15 ng/mL final concentration).
414 Pseudovirus was diluted 1:25 in media and added 1:1 to 110 µL of each antibody dilution.
415 Pseudovirus:antibody mixtures were incubated for 1 hour at 37°C. Media was removed from the Vero E6
416 cells and 50 µL of pseudovirus:antibody mixtures were added to the cells. One hour post-infection, 100
417 µL of media was added to wells containing pseudovirus:antibody mixtures and incubated for 17 hours at
418 37°C. Media was then removed and 100 µL of Bio-Glo reagent (diluted 1:1 in DPBS) was added to each

419 well. The plate was shaken on a plate shaker at 300 RPM at room temperature for 20 minutes and RLUs
420 were read on an EnSight plate reader. To control for background, the mean of the RLU values in
421 uninfected wells (n=6 per plate) was calculated and subtracted from all data points. Data were analyzed
422 and graphed using GraphPad Prism software (v8.4.1). The half maximal effective concentration (IC_{50})
423 values were calculated using a non-linear regression model (variable slope model, 4 parameters) of
424 log(inhibitor) versus response and the IC_{50} values were interpolated from the curve at y=50. The
425 geometric mean from at least two independent experiments was calculated in Excel (Version 16.36,
426 Microsoft). Fold change in IC_{50} relative to wild type was calculated for each experiment, and the mean
427 fold change was reported.

428 **Live virus neutralization.** VeroE6 cells were seeded into flat bottom 96-well plates at 20,000 cells/well
429 and cultured overnight at 37°C. Twenty-four hours later, 9-point 1:4 serial dilutions of antibody were
430 prepared in PBS and each dilution was tested in quadruplicate per plate (range: 25,600 to 0.390 ng/mL
431 final concentration). SARS-CoV-2 virus stock was diluted in infection media for a final concentration of
432 200 plaque forming units (PFU) per well. Antibody dilutions were added to the virus and incubated for 30
433 minutes at 37°C. Media was removed from the VeroE6 cells, mAb-virus complexes were added, and cells
434 were incubated at 37°C overnight. At 24 hours post-infection, cells were fixed with 250 µL 4% PFA,
435 incubated for 30 minutes at RT, then washed 3 times with PBS to remove residual PFA. The cells were
436 permeabilized with 50 µL of 0.125% Triton X-100 in PBS for 30 minutes at RT, followed by blocking
437 with 300 µL blocking buffer for 30 minutes at RT. The blocking buffer was removed, 50 µL of SARS-
438 CoV-2 nucleocapsid antibody at 1:3,000 in blocking buffer was added, and plate was incubated for 1 hour
439 at RT. Plates were washed 3 times with PBS and then incubated for 1 hour at RT with 50 µL/well of goat
440 anti-rabbit-Alexa647 secondary antibody at a final dilution of 1:3,000 in blocking buffer. After washing 5
441 times with PBS, 100 µL of fresh PBS was added for imaging. Plates were imaged on a Cytation5 plate
442 reader. Whole well images were acquired (12 images at 4X magnification per well) and nucleocapsid-
443 positive cells were counted using the manufacturer's software.

444 **Determination of Viral Titer by Focus-Forming Assay.** One day prior to infection, $1.2X10^4$ VeroE6
445 cells were plated in black-walled, clear bottomed 96-well plates. Virus samples were diluted 1:5 in
446 infection media and adsorbed onto VeroE6 cells for one hour at 37°C. The cells were washed once and
447 overlaid with 1% methylcellulose/serum-containing media. At 24 hours post-infection, the
448 methylcellulose overlay was removed, and cells were washed with PBS. Cells were fixed with 4% PFA,
449 incubated for 30 minutes at RT, then washed with PBS to remove residual PFA. The cells were
450 permeabilized with 50 µL of 0.25% Triton X-100 in PBS for 30 minutes at RT. The Triton X-100 was
451 removed, cells were washed twice with PBS, and incubated with 50 µL of SARS-CoV-2 nucleocapsid
452 antibody at 1:2,000 in blocking buffer for one hour at RT. Plates were washed three times with PBS and
453 then incubated for one hour at RT with 50 µL/well of goat anti-rabbit-Alexa647 secondary antibody at
454 1:1,000 in blocking buffer. After washing three times with PBS, 50 µL of Hoechst dye at 1:1,000 in PBS
455 was added for imaging. Plates were imaged on a Cytation5 plate reader. Whole well images were
456 acquired (12 images at 4X magnification per well) and nucleocapsid-positive foci were counted using the
457 manufacturer's software and used to determine focus-forming units/mL supernatant (FFU/mL).

458 **Determination of mAb-Dependent Activation of Human FcγRIIa, FcγRIIIa or FcγRIIb.** VIR-7831,
459 VIR-7832, S309-LS, and a control mAb with abrogated FcγR binding, S309-GRLR, were serially diluted
460 6-fold in assay buffer from 10,000 ng/ml to 0.006 ng/ml. Nine-point serial dilutions of mAbs were
461 incubated with 12,500 (for FcγRIIIa and FcγRIIb) or 10,000 (for FcγRIIa) CHO-CoV-2-Spike cells per
462 96-plate well in a white, flat-bottom plate for 15 minutes at room temperature. Jurkat effector cells
463 expressing indicated FcγRs and stably transfected with an NFAT-driven luciferase gene were thawed,
464 diluted in assay buffer, and added to the plate at an effector to target cell ratio of 6:1 for FcRγIIIa and
465 FcγRIIb or 5:1 for FcγIIa. Control wells were also included that were used to measure antibody-
466 independent activation (containing target cells and effector cells but no antibody) and background
467 luminescence of the plate (wells containing assay buffer only). Plates were incubated for 18 hours at 37°C
468 with 5% CO2. Activation of human FcγRs in this bioassay results in the NFAT-mediated expression of

469 the luciferase reporter gene. Luminescence was measured with a luminometer after adding the Bio
470 GloTM Luciferase Assay Reagent according to the manufacturer's instructions. To control for
471 background, the mean of the relative luminescence units (RLU) values in wells containing only Assay
472 Buffer was calculated and subtracted from all data points. Data were expressed as the average of RLUs
473 over the background

474 **Determination of NK-Cell Mediated Antibody-Dependent Cellular Cytotoxicity.** Primary NK cell
475 activation was tested using freshly isolated cells from two previously genotyped donors expressing
476 homozygous low affinity (F158) or high affinity (V158) FcγRIIIa. Serial dilutions of mAbs (serially
477 diluted 10-fold in AIM-V Medium from 40,000 ng/ml to 0.075 ng/ml) were incubated with 7,500 CHO-
478 CoV-2 Spike cells per well of a 96 well round-bottom plate for 10 minutes. Target cell and antibody
479 mixtures were then incubated with primary human NK cells as effectors at an effector-to-target ratio of
480 10:1. ADCC was measured using lactate dehydrogenase (LDH) release as a readout according to the
481 manufacturer's instructions (Cytotoxicity Detection Kit (LDH), Roche) after 4 hours of incubation at
482 37°C. In brief, plates were centrifuged for 4 minutes at 400 x g, and 35 µl of supernatant was transferred
483 to a flat 384 well plate. LDH reagent was prepared and 35 µl were added to each well. Using a kinetic
484 protocol, the absorbance at 490 nm and 650 nm was measured once every 2 minutes for 8 minutes, and
485 the slope of the kinetics curve was used as result. The percent specific lysis was determined by applying
486 the following formula: (specific release – spontaneous release) / (maximum release - spontaneous release)
487 x 100.

488 **Determination of Monocyte-Mediated Antibody-Dependent Cellular Phagocytosis.** ADCP assays
489 were performed using human PBMCs freshly isolated from whole blood. CHO CoV-2-Spike cells were
490 used as target cells and were fluorescently labeled with PKH67 Fluorescent Cell Linker Kit (Sigma
491 Aldrich) prior to incubation with mAbs, according to manufacturer's instructions. Serial dilutions of
492 mAbs (serially diluted 5-fold from 5,000 ng/ml to 0.32 ng/ml in RPMI-1640 + L-glutamine supplemented
493 with 10% Hyclone FBS + 2x anti-anti (antibiotic-antimycotic)) were incubated with 10,000 CHO-CoV-2-

494 Spike cells per well of a 96 well polypropylene plate for 10 minutes. Primary PBMCs were fluorescently
495 labeled with Cell Trace Violet according to the manufacturer's instructions. Target cell and antibody
496 mixtures were then incubated with labeled PBMCs at an effector-to-target ratio of 16:1. After an
497 overnight incubation at 37°C, monocytes were stained with anti-human CD14-APC antibody (BD
498 Pharmingen). Antibody-mediated phagocytosis was determined by flow cytometry, gating on CD14+
499 cells that were double positive for cell trace violet and PKH67. Raw data were exported from the flow
500 cytometer into the flow cytometry analysis software FlowJo v10 (Becton Dickinson) for gating and
501 determination of the percentage of $CD14^+$ cells that were also double positive for cell trace violet and
502 PKH67. Cells expressing only cell trace violet or only PKH67 were used to set the positive staining gates.

503 **In vitro resistance selection.** The selection of variants in the presence of increasing concentrations of
504 VIR-7832 was conducted in VeroE6 cells. The day before infection, 6 x 10^4 VeroE6 cells were seeded in
505 24 well plates and incubated overnight at 37°C. The next day, 600 focus forming units (FFU) of SARS-
506 CoV-2 virus (MOI = 0.01) was incubated with 0.5X IC_{50} of VIR-7832 (0.05 µg/mL) at 37°C for one hour
507 in infection media. The mAb-virus complexes were adsorbed on VeroE6 cells for one hour at 37°C in
508 duplicate wells. After adsorption, cells were washed with DMEM and overlaid with infection media
509 containing 0.05 µg/mL VIR-7832. Control wells infected without antibody were included with each
510 passage. Infected cells were monitored visually for CPE daily. In general, when infected cells exhibited ≥
511 50% CPE, the culture supernatants were harvested, diluted 1:200, and added to fresh VeroE6 cells in 24-
512 well plates with equivalent or increasing concentrations of VIR-7832. At each passage, supernatant was
513 aliquoted and frozen at -80°C for titer and neutralization analyses.

514 **In vitro assessment of potential for ADE.** VeroE6 cells were plated at 1.25X10^4 cells/well one day prior
515 to infection. For each independent experiment, moDCs and PBMCs from five unique moDC donors and
516 six unique PBMC donors were used, with three unique donors used for each independent experiment.
517 Cryopreserved monocytes from unique donors were differentiated into moDCs for six days using human
518 moDC differentiation media according to the manufacturer's protocol. Cryopreserved PBMCs from

519 unique donors are thawed in the presence 0.3 mg/mL DNase and cultured in media for one day prior to
520 infection. On the day of infection, moDCs, PBMCs, and U937 cells were counted and plated at $7.5X10^4$
521 cells/well.

522 To examine viral entry, 24 hours post-infection, cells were fixed with 4% PFA, incubated for 30 minutes
523 at RT, then washed with PBS to remove residual PFA. The cells were permeabilized with 50 µL of 0.25%
524 Triton X-100 in PBS for 30 minutes at RT. The Triton X-100 was removed, cells were washed twice with
525 PBS, and incubated with 50 µL of SARS-CoV-2 nucleocapsid antibody at 1:2,000 in blocking buffer for
526 one hour at RT. Plates were washed three times with PBS and then incubated for one hour at RT with 50
527 µL/well of goat anti-rabbit-Alexa647 secondary antibody at 1:1,000 in blocking buffer. After washing
528 three times with PBS, 50 µL of Hoechst dye at 1:1,000 in PBS was added for imaging. Plates were
529 imaged on a Cytation5 plate reader. Whole well images were acquired (12 images at 4X magnification
530 per well) and nucleocapsid-positive cells were counted using the manufacturer's software. The percent of
531 nucleocapsid+ cells was quantified using the Gen5 Imager software (Biotek, Vermont) as number of
532 Cy5+ cells, [(nucleocapsid+ cells)/number of Hoechst+ cells (total cells)]x100. Data was analyzed using
533 Prism v8.00 (GraphPad Software, La Jolla California USA, www.graphpad.com).

534 In order to quantify chemokines and cytokines from supernatants in a BSL2 laboratory, supernatants were
535 inactivated by 10 minutes exposure to UVC light at 5,000 µJ/cm2. Supernatants were diluted 1:5 in
536 infection media and levels of cytokines/chemokines were quantified using the U-plex 96-well assay
537 according to the manufacturer's protocol (Meso Scale Diagnostics, Rockville, MD). Quantification of
538 cytokines and chemokines were determined based on an 8-point standard curve in duplicate, provided by
539 the manufacturer. Cytokine data was analyzed using the Discovery Workbench v4.0.13 software (Meso
540 Scale Diagnostics). Data was graphed and statistical analyses were conducted using Prism software.

541 **Sequencing of SARS-CoV-2 Spike Gene.** To isolate nucleic acid from the supernatant of viral passages,
542 120 µL of cell supernatant was added to 360 µL of Trizol and stored at -80°C for further analysis. Trizol
543 collected samples from viral passages where a shift in neutralization > 2-fold relative to wild type was

544 detected were subjected to RNA isolation using PureLink RNA Mini Kit with the incorporation of on-
545 column PureLink DNase Treatment, following manufacturer's instructions. Reverse transcription
546 reactions were performed with 6 µL of purified RNA and oligoT primers using the NEB ProtoScript II
547 First Strand cDNA Synthesis kit, according to manufacturer's instructions. The resulting cDNA was used
548 as a template for PCR amplification of the spike gene using the KapaBiosystems polymerase (KAPA HiFi
549 HotStart ReadyMix) with primers 5' aattatcttggcaaaccacg-3' and 5' tgaggcttgtatcggtatcg-3'.
550 Amplification conditions included an initial 3 minutes at 95°C, followed by 28 cycles with 20 seconds at
551 98°C, 15 seconds at 62°C and 72°C for 2 minutes, with a final 4 minutes at 72°C. PCR products were
552 purified using AMPure XP beads following manufacturer's instructions. The size of the amplicon was
553 confirmed by analyzing 2 µL of PCR products using the Agilent D5000 ScreenTape System. Products
554 were quantified by analyzing 1 µL with the Quant-iT dsDNA High-Sensitivity Assay Kit. Twenty ng of
555 purified PCR product was used as input for library construction using the NEBNext Ultra II FS DNA
556 Library Prep kit following manufacturer's instructions. DNA fragmentation was performed for 13
557 minutes. NEBNext Multiplex Oligos for Illumina Dual Index Primer Set 1 was used for library
558 construction, with a total of 6 PCR cycles. Libraries size was determined using the Agilent D1000
559 ScreenTape System and quantified with the Quant iT dsDNA High-Sensitivity Assay Kit. Equal amounts
560 of each library were pooled together for multiplexing and 'Protocol A: Standard Normalization Method'
561 of the Illumina library preparation guide was used to prepare 8 pM final multiplexed libraries with 1%
562 PhiX spike-in for sequencing. The MiSeq Reagent Kit v3 (600-cycle) was used for sequencing the
563 libraries on the Illumina MiSeq platform, with 300 cycles for Read 1, 300 cycles for Read 2, 8 cycles for
564 Index 1, and 8 cycles for Index 2.

565 **Bioinformatics Analysis of Conservation.** Available genome sequences for SARS-CoV-2 were
566 downloaded from Global Initiative on Sharing All Influenza Data (GISAID; https://www.gisaid.org/) on
567 February 26, 2021. Bat and pangolin sequences were removed to yield human-only sequences. The spike
568 open reading frame was localized by aligning the reference protein sequence (NCBI reference sequence:

569 YP_009724390.1) to the genomic sequence of isolates with Exonerate v.2.4.0. Coding nucleotide
570 sequences were translated in silico using seqkit v.0.12.0. Multiple sequence alignment was performed
571 using MAFFT v.7.455. Variants were determined by comparison of aligned sequences to the reference
572 sequence using the R v3.6.3/Bioconductor v.3.10 package Biostrings v.2.54.0.

573 **In vivo studies.** Syrian golden hamster studies were conducted at Lovelace Biomedical (Albuquerque,
574 NM). Twelve- to sixteen-week-old male hamsters were interperitoneally administered a non-LS version
575 of VIR-7831 (SGHmAb-no-LS), control antibody or diluent Day -1 or Day -2 prior to virus challenge.
576 Animals were inoculated intranasally at Day 0 with $7.4x10^4$ $TCID_{50}$ with SARS-CoV-2 (isolate USA-
577 WA1/2020). Animals were also weighed once daily in the morning beginning on study Day -10 and
578 continuing until the end of the study. Following euthanasia, RT-qPCR was performed on lung
579 homogenates using quantitative real-time PCR methods targeting the SARS-CoV-2 N gene and the
580 median tissue culture infections dose ($TCID_{50}$) was determined per Lovelace internal methodology.

581 **Author Contributions**

582 Conceived studies: A.L.C, C.H-D., F.A.P, D.M., M.S., L.S., A.T., S.H., G.S., H.W.V., D.C., C.M.H. Designed
583 studies and experiments: A.L.C, C.H.D., F.A.P, D.M., M.S., M.L.A., B.G., J.D., L.R.,A.C., J.W., N.C., E.C.,
584 S.L., C.C., L.S., A.T., S.H., G.S., H.W.V., D.C., C.M.H. Performed experiments: D.M., M.S., M.L.A., B.G., J.D.,
585 L.R., H.T., J.D., S.S., B.S., S.B., J.W., J.Z., H.K., A.C., M.M-R., N.C., E.C. Analyzed and interpreted data: A.L.C.,
586 C.H-D., F.A.L., D.M., M.S., M.L.A., B.G., J.D., L.R., H.T., B.S., S.B., J.W., J.Z., H.K., A.C., M. M-R., N.C., E.C.,
587 S.L., C.C., L.S., A.T., S.H., G.S., H.W.G, D.C., C.M.H. Prepared the manuscript with input from all authors:
588 A.L.C., G.S., A.T., D.C., H.W.G., C.M.H.

589 **Competing interests**

590 All authors are current employees of Vir Biotechnology or Humabs BioMed SA (a fully-owned subsidiary
591 of Vir Biotechnology) and may hold shares in Vir Biotechnology. H.W.V. is a founder of PierianDx and
592 Casma Therapeutics.

593

REFERENCES

1. WHO Coronavirus Disease (COVID-19) Dashboard | WHO Coronavirus Disease (COVID-19) Dashboard. *undefined* https://covid19.who.int/.

2. Levin, A. T. *et al.* Assessing the age specificity of infection fatality rates for COVID-19: systematic review, meta-analysis, and public policy implications. *Eur J Epidemiol* **35**, 1123–1138 (2020).

3. Dennis, A. *et al.* Multi-organ impairment in low-risk individuals with long COVID. doi:10.1101/2020.10.14.20212555.

4. Murphy, J. *et al.* Psychological characteristics associated with COVID-19 vaccine hesitancy and resistance in Ireland and the United Kingdom. *Nat Commun* **12**, 29 (2021).

5. Khubchandani, J. *et al.* COVID-19 Vaccination Hesitancy in the United States: A Rapid National Assessment. *J Commun Health* 1–8 (2021) doi:10.1007/s10900-020-00958-x.

6. Sallam, M. *et al.* High Rates of COVID-19 Vaccine Hesitancy and Its Association with Conspiracy Beliefs: A Study in Jordan and Kuwait among Other Arab Countries. *Nato Adv Sci Inst Se* **9**, 42 (2021).

7. Tegally, H. *et al.* Emergence and rapid spread of a new severe acute respiratory syndrome-related coronavirus 2 (SARS-CoV-2) lineage with multiple spike mutations in South Africa. *medRxiv* (2020) doi:10.1101/2020.12.21.20248640.

8. Naveca, F. *et al.* Phylogenetic relationship of SARS-CoV-2 sequences from Amazonas with emerging Brazilian variants harboring mutations E484K and N501Y in the Spike protein - SARS-CoV-2 coronavirus / nCoV-2019 Genomic Epidemiology - Virological. https://virological.org/t/phylogenetic-relationship-of-sars-cov-2-sequences-from-amazonas-with-emerging-brazilian-variants-harboring-mutations-e484k-and-n501y-in-the-spike-protein/585 (2011).

9. Rambaut, A. *et al.* Preliminary genomic characterisation of an emergent SARS-CoV-2 lineage in the UK defined by a novel set of spike mutations - SARS-CoV-2 coronavirus / nCoV-2019 Genomic Epidemiology - Virological. https://virological.org/t/preliminary-genomic-characterisation-of-an-emergent-sars-cov-2-lineage-in-the-uk-defined-by-a-novel-set-of-spike-mutations/563 (2020).

10. Bamlanivimab EUA Letter of Authorization Reissue 02092021. https://www.fda.gov/media/143603/download.

11. Casirivimab and Imdevimab EUA Fact Sheet for Healthcare Providers. https://www.fda.gov/media/143892/download.

628 12. Lilly's neutralizing antibody bamlanivimab (LY-CoV555) prevented COVID-19 at nursing
629 homes in the BLAZE-2 trial, reducing risk by up to 80 percent for residents.
630 https://investor.lilly.com/node/44291/pdf.

631 13. Gottlieb, R. L. *et al.* Effect of Bamlanivimab as Monotherapy or in Combination With
632 Etesevimab on Viral Load in Patients With Mild to Moderate COVID-19. *Jama* **325**, 632–644
633 (2021).

634 14. Chen, P. *et al.* SARS-CoV-2 Neutralizing Antibody LY-CoV555 in Outpatients with Covid-
635 19. *New Engl J Med* (2020) doi:10.1056/nejmoa2029849.

636 15. Weinreich, D. M. *et al.* REGN-COV2, a Neutralizing Antibody Cocktail, in Outpatients with
637 Covid-19. *New Engl J Med* **384**, 238–251 (2020).

638 16. Starr, T. N. *et al.* Prospective mapping of viral mutations that escape antibodies used to treat
639 COVID-19. *Science* **371**, 850–854 (2021).

640 17. Wang, P. *et al.* Increased Resistance of SARS-CoV-2 Variants B.1.351 and B.1.1.7 to
641 Antibody Neutralization. *Biorxiv* 2021.01.25.428137 (2021) doi:10.1101/2021.01.25.428137.

642 18. Schäfer, A. *et al.* Antibody potency, effector function, and combinations in protection and
643 therapy for SARS-CoV-2 infection in vivo. *J Exp Med* **218**, (2020).

644 19. Winkler, E. S. *et al.* Human neutralizing antibodies against SARS-CoV-2 require intact Fc
645 effector functions and monocytes for optimal therapeutic protection. *Biorxiv* 2020.12.28.424554
646 (2020) doi:10.1101/2020.12.28.424554.

647 20. Bournazos, S. & Ravetch, J. V. Fcγ Receptor Function and the Design of Vaccination
648 Strategies. *Immunity* **47**, 224–233 (2017).

649 21. Pinto, D. *et al.* Cross-neutralization of SARS-CoV-2 by a human monoclonal SARS-CoV
650 antibody. *Nature* **583**, 290–295 (2020).

651 22. Pinto, D. *et al.* Cross-neutralization of SARS-CoV-2 by a human monoclonal SARS-CoV
652 antibody. *Nature* **583**, 290–295 (2020).

653 23. Ko, S.-Y. *et al.* Enhanced neonatal Fc receptor function improves protection against primate
654 SHIV infection. *Nature* **514**, 642 (2014).

655 24. Zalevsky, J. *et al.* Enhanced antibody half-life improves in vivo activity. *Nat Biotechnol* **28**,
656 157 (2010).

657 25. Gaudinski, M. R. *et al.* Safety and pharmacokinetics of the Fc-modified HIV-1 human
658 monoclonal antibody VRC01LS: A Phase 1 open-label clinical trial in healthy adults. *Plos Med*
659 **15**, e1002493 (2018).

660 26. Bournazos, S., Corti, D., Virgin, H. W. & Ravetch, J. V. Fc-optimized antibodies elicit CD8
661 immunity to viral respiratory infection. *Nature* 1–9 (2020) doi:10.1038/s41586-020-2838-z.

662 27. Weitzenfeld, P., Bournazos, S. & Ravetch, J. V. Antibodies targeting sialyl Lewis A mediate
663 tumor clearance through distinct effector pathways. *J Clin Invest* **129**, 3952–3962 (2019).

664 28. Bournazos, S., Corti, D., Virgin, H. W. & Ravetch, J. V. Fc-optimized antibodies elicit CD8
665 immunity to viral respiratory infection. *Nature* 1–9 (2020) doi:10.1038/s41586-020-2838-z.

666 29. Diamond, M. *et al.* SARS-CoV-2 variants show resistance to neutralization by many
667 monoclonal and serum-derived polyclonal antibodies. *Res Square* (2021) doi:10.21203/rs.3.rs-
668 228079/v1.

669 30. Chen, R. E. *et al.* Resistance of SARS-CoV-2 variants to neutralization by monoclonal and
670 serum-derived polyclonal antibodies. *Nat Med* 1–10 (2021) doi:10.1038/s41591-021-01294-w.

671 31. Kallewaard, N. L. *et al.* Structure and Function Analysis of an Antibody Recognizing All
672 Influenza A Subtypes. *Cell* **166**, 596–608 (2016).

673 32. DiLillo, D. J., Tan, G. S., Palese, P. & Ravetch, J. V. Broadly neutralizing hemagglutinin
674 stalk–specific antibodies require FcγR interactions for protection against influenza virus in vivo.
675 *Nat Med* **20**, 143–151 (2014).

676 33. Dunand, C. J. H. *et al.* Both Neutralizing and Non-Neutralizing Human H7N9 Influenza
677 Vaccine-Induced Monoclonal Antibodies Confer Protection. *Cell Host Microbe* **19**, 800–813
678 (2016).

679 34. Leon, P. E. *et al.* Optimal activation of Fc-mediated effector functions by influenza virus
680 hemagglutinin antibodies requires two points of contact. *Proc National Acad Sci* **113**, E5944–
681 E5951 (2016).

682 35. Bruhns, P. *et al.* Specificity and affinity of human Fcγ receptors and their polymorphic
683 variants for human IgG subclasses. *Blood* **113**, 3716–3725 (2009).

684 36. Weitzenfeld, P., Bournazos, S. & Ravetch, J. V. Antibodies targeting sialyl Lewis A mediate
685 tumor clearance through distinct effector pathways. *J Clin Invest* **129**, 3952–3962 (2019).

686 37. Cheng, Z. J. *et al.* Development of a robust reporter-based ADCC assay with frozen, thaw-
687 and-use cells to measure Fc effector function of therapeutic antibodies. *J Immunol Methods* **414**,
688 69–81 (2014).

689 38. Arvin, A. M. *et al.* A perspective on potential antibody-dependent enhancement of SARS-
690 CoV-2. *Nature* 1–11 (2020) doi:10.1038/s41586-020-2538-8.

691 39. Joyner, M. J. & Wright, R. S. Safety Update: CO VID-19 Convalescent Plasma in
692 20,000 Hospitalized Patients. *Mayo Clinic Proceedings* (2020).

693 40. Arvin, A. M. *et al.* A perspective on potential antibody-dependent enhancement of SARS-
694 CoV-2. *Nature* **584**, 353–363 (2020).

695 41. Khurana, S. *et al.* Vaccine-induced anti-HA2 antibodies promote virus fusion and enhance
696 influenza virus respiratory disease. *Sci Transl Med* **5**, 200ra114 (2013).

697 42. Winarski, K. L. *et al.* Antibody-dependent enhancement of influenza disease promoted by
698 increase in hemagglutinin stem flexibility and virus fusion kinetics. *Proc National Acad Sci* **116**,
699 15194–15199 (2019).

700 43. Hui, K. P. Y. *et al.* Tropism, replication competence, and innate immune responses of the
701 coronavirus SARS-CoV-2 in human respiratory tract and conjunctiva: an analysis in ex-vivo and
702 in-vitro cultures. *Lancet Respir Medicine* (2020) doi:10.1016/s2213-2600(20)30193-4.

703 44. Liu, Z. *et al.* Identification of Common Deletions in the Spike Protein of Severe Acute
704 Respiratory Syndrome Coronavirus 2. *J Virol* **94**, (2020).

705 45. Baum, A. *et al.* Antibody cocktail to SARS-CoV-2 spike protein prevents rapid mutational
706 escape seen with individual antibodies. *Science* **369**, 1014–1018 (2020).

707 46. Thomson, E. C. *et al.* Circulating SARS-CoV-2 spike N439K variants maintain fitness while
708 evading antibody-mediated immunity. *Cell* (2021) doi:10.1016/j.cell.2021.01.037.

709 47. Starr, T. N., Greaney, A. J., Dingens, A. S. & Bloom, J. D. Complete map of SARS-CoV-2
710 RBD mutations that escape the monoclonal antibody LY-CoV555 and its cocktail with LY-
711 CoV016. doi:10.1101/2021.02.17.431683.

712 48. Wise, J. Covid-19: The E484K mutation and the risks it poses. *Bmj* **372**, n359 (2021).

713 49. VIR-7831 for the Early Treatment of COVID-19 in Outpatients - Full Text View -
714 ClinicalTrials.gov. https://clinicaltrials.gov/ct2/show/NCT04545060?term=VIR-
715 7831&draw=2&rank=2.

716 50. A Study of Immune System Proteins in Participants With Mild to Moderate COVID-19
717 Illness - Full Text View - ClinicalTrials.gov.
718 https://clinicaltrials.gov/ct2/show/NCT04634409?term=VIR-7831&draw=2&rank=3.

719 51. Vir Biotechnology and GSK announce NHS-supported AGILE study to evaluate VIR-7832
720 in the early treatment of COVID-19 | GSK. *undefined* https://www.gsk.com/en-gb/media/press-
721 releases/vir-biotechnology-and-gsk-announce-nhs-supported-agile-study-to-evaluate-vir-7832-
722 in-the-early-treatment-of-covid-19/.

723 52. Wise, J. Covid-19: New coronavirus variant is identified in UK. *Bmj* **371**, m4857 (2020).

724 53. CoVariants. https://covariants.org/.

725 54. Piccoli, L. *et al.* Mapping neutralizing and immunodominant sites on the SARS-CoV-2 spike
726 receptor-binding domain by structure-guided high-resolution serology. *Cell* (2020)
727 doi:10.1016/j.cell.2020.09.037.

728 55. Rappazzo, C. G. *et al.* Broad and potent activity against SARS-like viruses by an engineered
729 human monoclonal antibody. *Science* **371**, 823–829 (2021).

730 56. Sette, A. & Crotty, S. Adaptive immunity to SARS-CoV-2 and COVID-19. *Cell* **184**, 861–
731 880 (2021).

732 57. Stettler, K. *et al.* Specificity, cross-reactivity and function of antibodies elicited by Zika virus
733 infection. *Science* **353**, aaf8505 (2016).

734

735 **FIGURE LEGENDS**

736 **Figure 1.** VIR-7831 and VIR-7831 bind S and neutralize SARS-CoV-2 virus and S variants of concern in
737 vitro. a) Binding of VIR-7831 (black circles) and VIR-7832 (blue squares) to SARS-CoV-2 RBD was
738 tested by ELISA. Shown is the average of four replicates and SD derived from three independent
739 experiments. b) Association and dissociation profiles of VIR-7831 to SARS-CoV-2-RBD were measured
740 using SPR. The double reference subtracted curves (shown for single replicates) are plotted together with
741 the curve fit in black (obscured by close overlay with the data). Values are from two independent
742 experiments. c) Binding of VIR-7831 (black circles) and VIR-7832 (blue squares) to cell-surface S
743 protein was determined by flow cytometry. Data are expressed as the percentage of the positive cells.
744 Results shown are from one experiment and representative of three independent experiments performed.
745 d) In vitro neutralization of live wildtype SARS-CoV-2 by different concentrations of VIR-7831 (black
746 circles) and VIR-7832 (blue squares) measured by nucleocapsid staining 24-hours post-infection. Results
747 shown are from one experiment and representative of at least three independent experiments performed.
748 e) Neutralization of VSV pseudotyped virus expressing S variants of concern in a VeroE6 assay. Results
749 shown are from one experiment and representative of at least two independent experiments performed.

750 **Figure 2.** VIR-7831 and VIR-7832 demonstrate effector function in vitro. In vitro effector function (a-e)
751 activation profiles of human FcγRIIa (a), FcγRIIb (b), FcγRIIIa low-affinity (F158) (c) or FcγRIIIa high-
752 affinity binding allele (V158) (d) using bioreporter assays using S-expressing CHO cells as the target
753 antigen. Data points show means± SD of duplicates. NK-cell mediated killing (ADCC) of S-expressing
754 CHO cells using freshly isolated cells from two donors previously genotyped for homozygous expression
755 of low-affinity (F/F158) (e) or high-affinity (V/V158) FcγRIIIa (f). Data points are means of
756 quadruplicates ± SD. g) Antibody-dependent cellular phagocytosis (ADCP) using S-expressing CHO cells
757 and freshly isolated PBMCs. Data represent the means of duplicates ± SD.

758 **Figure 3.** VIR-7831 shows in vivo efficacy in a hamster SARS-CoV-2 model of infection. a) Overview
759 of hamster in vivo study design. b) and c) Animal weight over time as a percent of starting weight in
760 animals dosed a Day -1 (b) or Day -1 (c). Medians of at least N=6 animals and interquartile range are
761 shown. d) and e) Day 4 terminal weights expressed as a percentage of starting weight for animals dosed at
762 Day -1 (d) or Day -2 (e). Bar denotes median values. f) and g) Day 4 lung viral load in Day -1 (f) or Day -
763 2 (g) treated animals as assessed by RT-qPCR. Bar denotes median values. h) and i) infectious virus in
764 lung at Day 4 for Day -1 (h) or Day -2 (i) dosed animals. Bar denotes median values. ns=not significant,
765 ** = $p<0.05$, and *** = <0.005 as assessed by the Mann-Whitney U-test.

766 **Table 1.** VIR-7831 and VIR-7832 retain activity against S variants of concern**.** Average fold change in
767 VIR-7831 and VIR-7832 IC_{50} compared to relative wild-type controls for S variants tested in a
768 VSV/VeroE6 pseudotyped virus system. Data shown are averages of at least two independent
769 experiments.

770 **Table 2.** VIR-7831 and VIR-7832 retain activity against variants that confer resistance to authorized
771 mAbs. Activity of VIR-7831 against variants conferring reduced susceptibility to bamlanivimab,
772 imdevimab or casirivimab in a VSV/VeroE6 pseudotyped virus system. The geometric mean of IC_{50}s and
773 average fold-change versus the relative wild-type control from at least two independent experiments are
774 shown.

775 **Table 3.** The VIR-7831/VIR-7832 epitope is highly conserved. Conservation data comprising >540,000
776 sequences from the GISAID database and variants at each position are shown. Variants in bold were
777 tested in a pseudotyped virus assay.

778 **Table 4.** Activity of VIR-7831 against epitope variants. VIR-7831/VIR-7832 epitope variants detected in
779 sequences from the GISAID database were tested in a VSV/VeroE6 pseudotyped virus system. The
780 geometric mean of IC_{50}s and average fold-change versus the relative wild-type control from at least two
781 independent experiments are shown.

782 **Supplemental Figure 1.** Binding of VIR-7831 and VIR-7832 to human FcγRs and C1q as measured by
783 SPR. Binding of VIR-7831 and VIR-7832 to a) human FcγRIIa (H131 and R131 alleles), FcγRIIIa (F158
784 and V158 alleles) and FcγRIIb were measured using SPR. Biotinylated purified FcγRs were captured on
785 the sensor chip surface prior to injection of VIR-7831 or VIR-7832. Association and dissociation profiles
786 (separated by the vertical dotted line) were measured in real time as change in the SPR signal. b) Binding
787 of VIR-7831 and VIR-7832 to complement component C1q was measured using BLI on an Octet Red96
788 instrument. Association and dissociation profiles (separated by the vertical dotted line) were measured in
789 real time as change in the interference pattern.

790 **Supplemental Figure 2.** Sub-neutralizing concentrations of VIR-7831 and VIR-7832 do not enhance
791 viral entry, viral replication or cytokine production in vitro. Internalization (a) and replication (b) of
792 SARS-CoV-2 was evaluated in VeroE6, moDCs or PBMCs at various timepoints. Two independent
793 experiments with human moDCs and PBMCs from three individual donors were analyzed (5 unique
794 moDC donors, 6 unique PBMC donors total between two experiments). VeroE6 cells were run in
795 duplicate for both independent experiments. Data from each replicate well from two independent
796 experiments are plotted as individual points, with horizontal lines representing the median. Mann-
797 Whitney U-test comparison to no antibody group, *$p<0.05$. c) Supernatant cytokine and chemokine levels
798 as measured by MSD at the indicated time post infection. Data from two independent experiments (three
799 replicates each, five unique donors) are plotted as the mean and SD.

800 **Supplemental Figure 3.** Overview of VIR-7832 resistance selection method. All passaging was
801 conducted in duplicate wells. (a) VIR-7832 concentration was increased during each passage. P3 X
802 indicates passage 3 virus, after which virus was lost with subsequent increases in concentration. In (b) and
803 (c), p3X denotes where passage 3 virus from (a) was used to initiate (b) viral lineage 1 and (c) viral
804 lineage 2. Arrows indicate passages that were subjected to sequence analysis, and * indicate the passages
805 in lineage 1 with no detectable virus or CPE. Selection continued for a total of eight passages.

806 **Supplemental Table 1.** Amino acid substitutions identified in the SARS-CoV-2 S upon in vitro selection
807 with VIR-7832. Spike gene sequences were compared to a SARS-CoV-2 reference sequence (NCBI:
808 NC_045512.2) to identify variants. Fold-changes in IC_{50} were determined compared to the SARS-CoV-2
809 virus stock.

810 **Supplemental Table 2.** VIR-7831 and VIR-7832 activity against selected S variants. VIR-7831/VIR-
811 7832 epitope variants observed by in vitro resistance selection were individually tested in a VSV/VeroE6
812 pseudotyped virus system. The geometric mean of IC_{50}s and average fold-change versus the relative wild-
813 type control from at least two independent experiments are shown.

814

Figure 1

a)

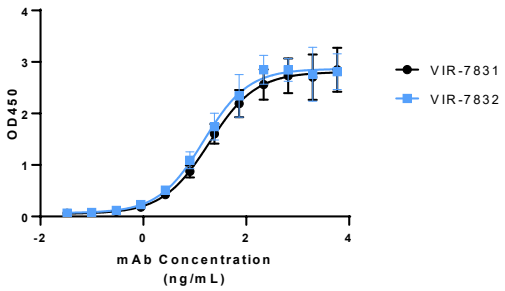

b)

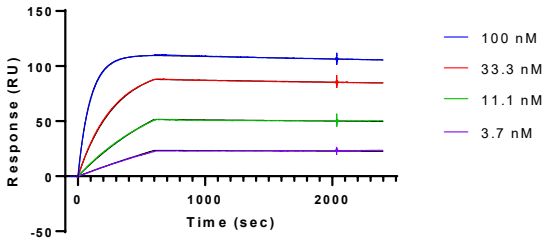

c)

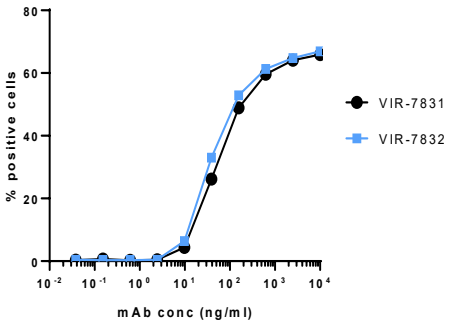

d)

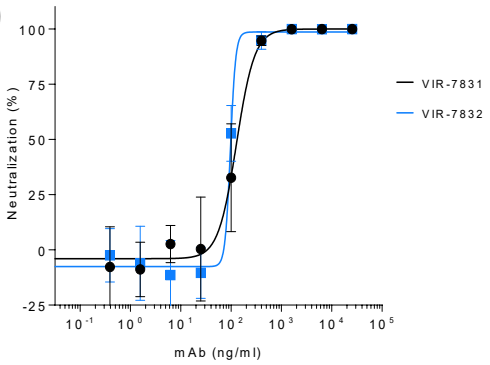

e)

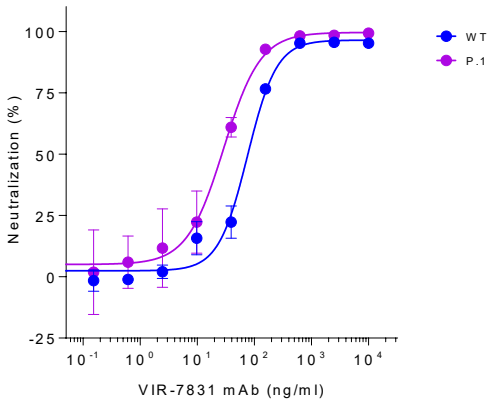

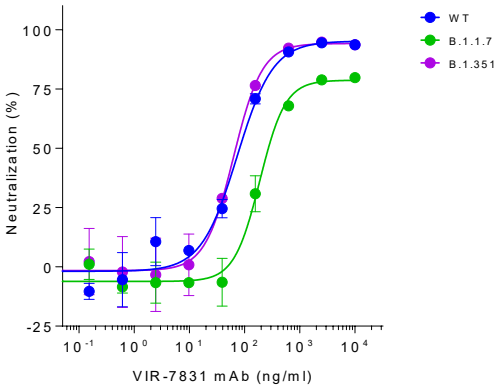

f)

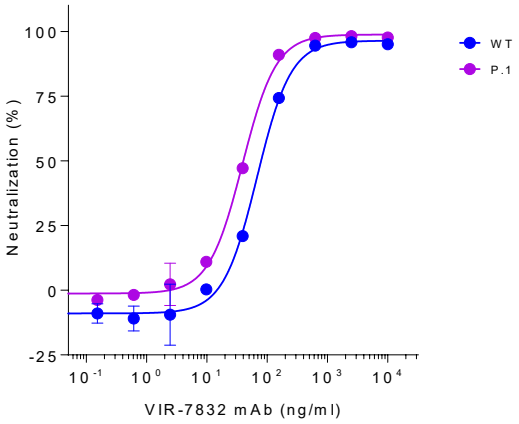

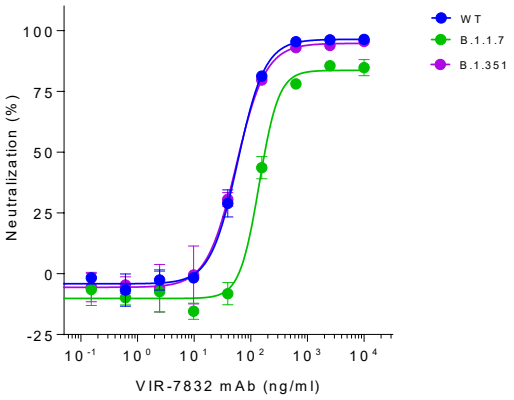

Figure 2

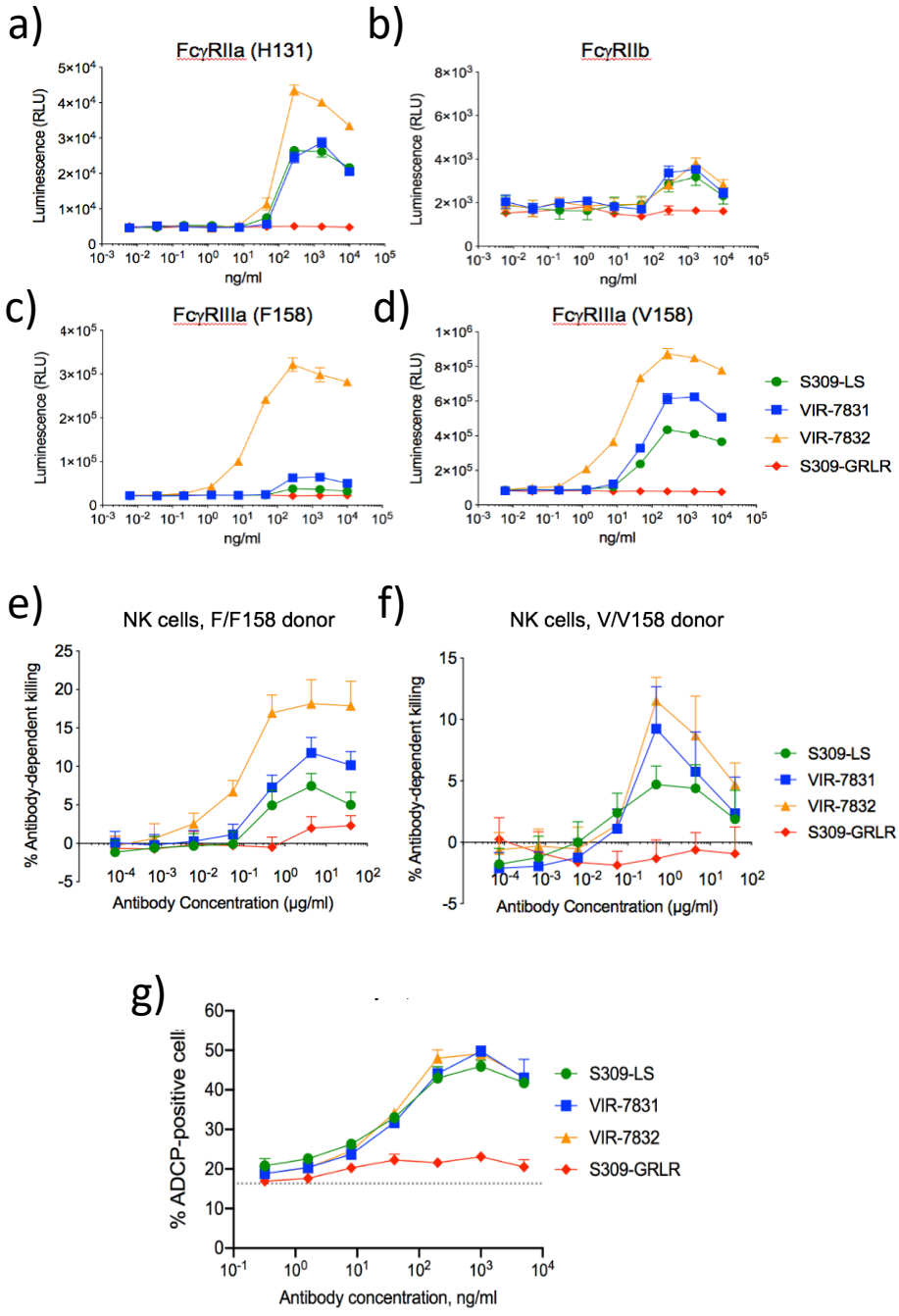
a)
FcγRIIa (H131)
Luminescence (RLU)
ng/ml
b)
FcγRIIb
Luminescence (RLU)
ng/ml
c)
FcγRIIIa (F158)
Luminescence (RLU)
ng/ml
d)
FcγRIIIa (V158)
Luminescence (RLU)
ng/ml
S309-LS
VIR-7831
VIR-7832
S309-GRLR
e)
NK cells, F/F158 donor
% Antibody-dependent killing
Antibody Concentration (μg/ml)
f)
NK cells, V/V158 donor
% Antibody-dependent killing
Antibody Concentration (μg/ml)
S309-LS
VIR-7831
VIR-7832
S309-GRLR
g)
% ADCP-positive cell
Antibody concentration, ng/ml
S309-LS
VIR-7831
VIR-7832
S309-GRLR

Figure 3

a)

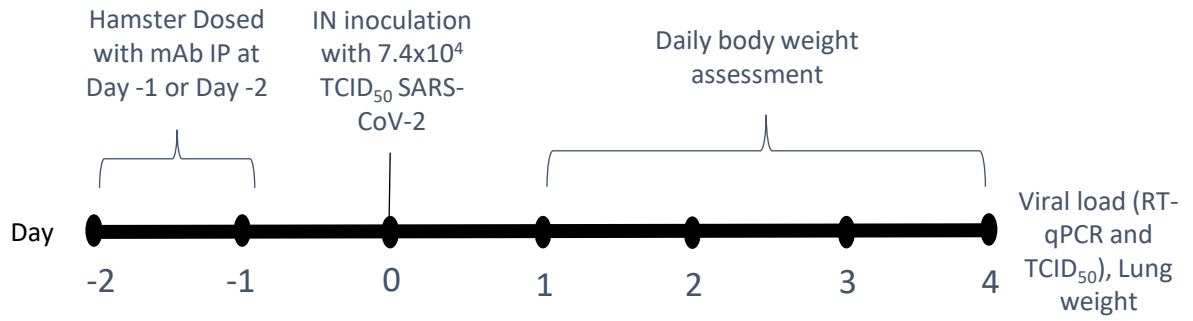

b)

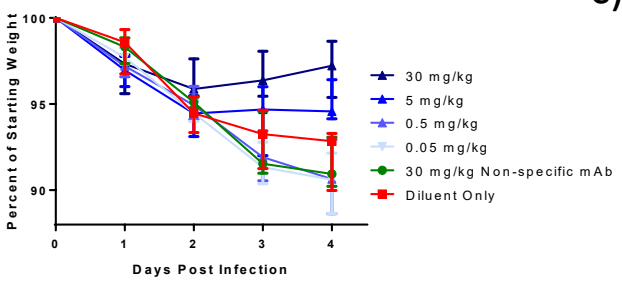

c)

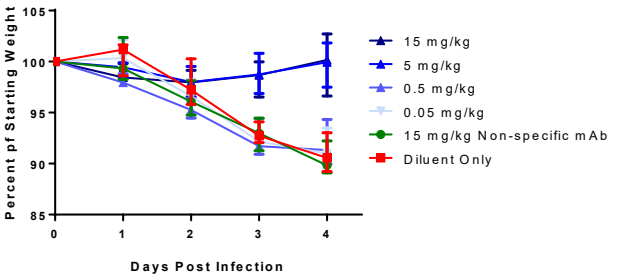

d)

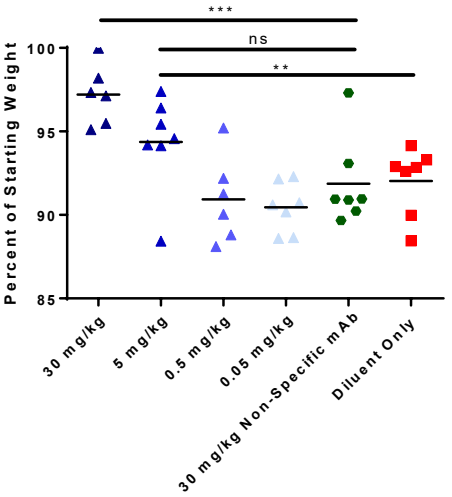

e)

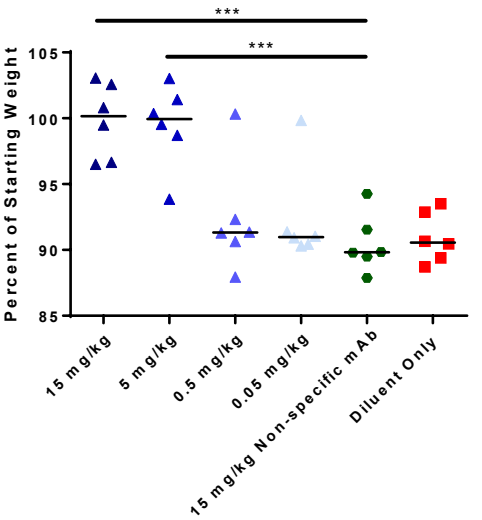

f)

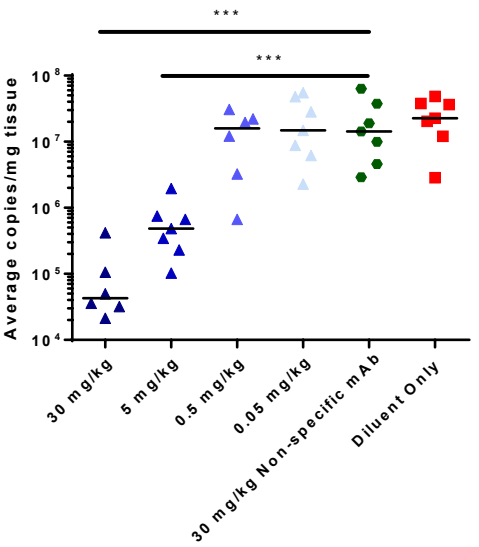

g)

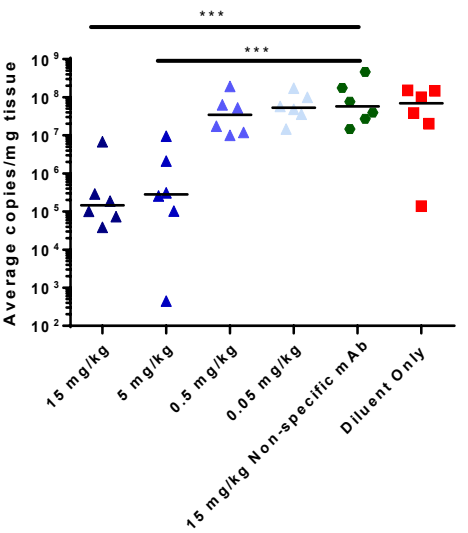

h)

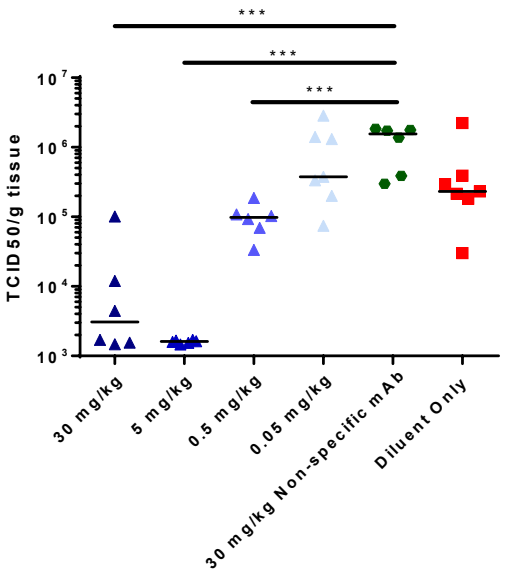

i)

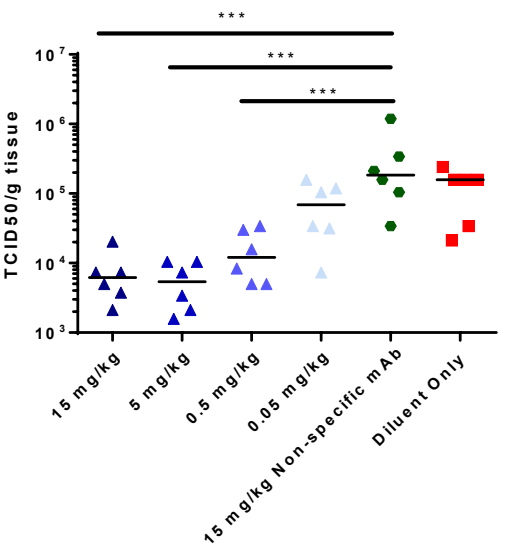

Table 1

SARS-CoV-2 Variant Name	Variants in Tested Spike Sequence	Average Fold Change in IC_{50} Compared to Relative Wild-Type	
		VIR-7831	VIR-7832
B.1.1.7 (UK)	H69-, V70-, Y144-, N501Y, A570D, D614G, P681H, T716I, S982A, D1118H	2.30	2.50
B.1.351 (SA)	L18F, D80A, D215G, R246I, K417N, E484K, N501Y, D614G, A701V	0.60	0.72
P.1 (Brazil)	D138Y, D614G, E484K, H655Y, K417T, L18F, N501Y, P26S, R190S, T1027I, T20N, V1176F	0.35	0.42

Table 2

Amino acid position	Substitution / deletion	mAb with reduced susceptibility	Variants in Tested Spike Sequence	Average Fold Change in IC_{50} Compared to Relative Wild-Type
E406	W	casirivimab+ imdevimab	E406W	0.74
K417	E	casirivimab	K417E	0.89
N439	K	imdevimab	N439K, D614G	0.86
N440	D	imdevimab	N440D	1.29
K444	Q	imdevimab	K444Q	1.11
V445	A	imdevimab	V445A	3.38
G446	V/I	imdevimab	G446V, D614G	1.50
Y453	F	casirivimab	G261D, Y453F	2.19
L455	F	casirivimab	L455F, D614G	0.56
G476	S	casirivimab	G476S	2.94
E484	K	bamlanivimab	E484K, D614G	0.33
F486	V/I	casirivimab	F486V	1.10
Y489	H	casirivimab	Y489H	1.48
F490	S	bamlanivimab	F490S	0.85
Q493	K	casirivimab, bamlanivimab	Q483K	0.98
S494	P	casirivimab, bamlanivimab	S494P, D614G	2.50

Table 3

Amino Acid Position	Reference Amino Acid	Variants Identified	Percent Reference AA Conservation
333	T	I, K	>99.99
334	N	**K**	>99.99
335	L	**F**, S	>99.99
336	C	S	>99.99
337	P	**S, T, L, H, R**	>99.99
339	G	**D**, S, F, V	99.98
340	E	**A, K, G**, D, Q	99.99
341	V	**I**, A	99.99
343	N	-	100
344	A	**S**, T, V, P	99.96
345	T	I, S	>99.99
346	R	**K**, S, I, T, G	99.97
354	N	**D, K, S**, H	99.96
356	K	R, M, N, T	99.99
357	R	K	99.98
358	I	L, T, V	> 99.99
359	S	**N**, R, T, G	99.98
360	N	S, T, Y	> 99.99
361	C	T	> 99.99
440	N	**K**, Y, S, D, T, H	99.96
441	L	I, F, R, V	> 99.99
509	R	K, T	> 99.99

AA: Amino acid

Table 4

Epitope Reference Amino Acid	**Amino Acid Changes in Spike protein**	**Average Fold-Change IC_{50} Relative to Wild-Type**
N334	N334K, D614G	1.27
L335	L335F	0.81
P337	P337H, D614G[a]	7.50
	P337L, D614G[a]	180.46
	P337R, D614G[a]	>276
	P337S, D614G	1.26
	P337T, D614G[a]	5.38
G339	G339D, D614G	1.18
E340	E340A	>100
	E340K	>297
	E340G, D614G[a]	27.47
V341	V341I, D614G	0.16
A344	A344S	0.89
R346	R346K, D614G	0.72
N354	N354D	1.00
	N354K, T95I	0.76
	N354S, D614G	0.89
S359	S359N	0.96
N440	N440K, D614G	0.48

Supplemental Figure 1

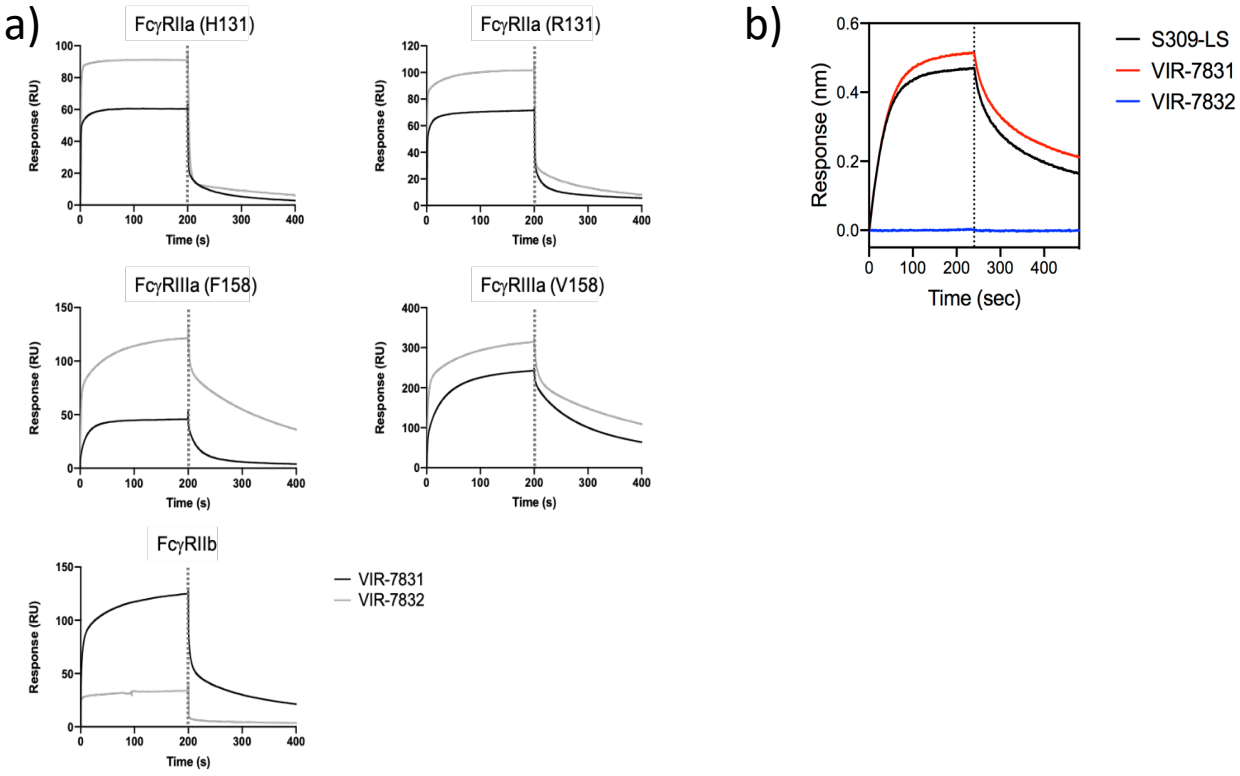

Supplemental Figure 2

a)

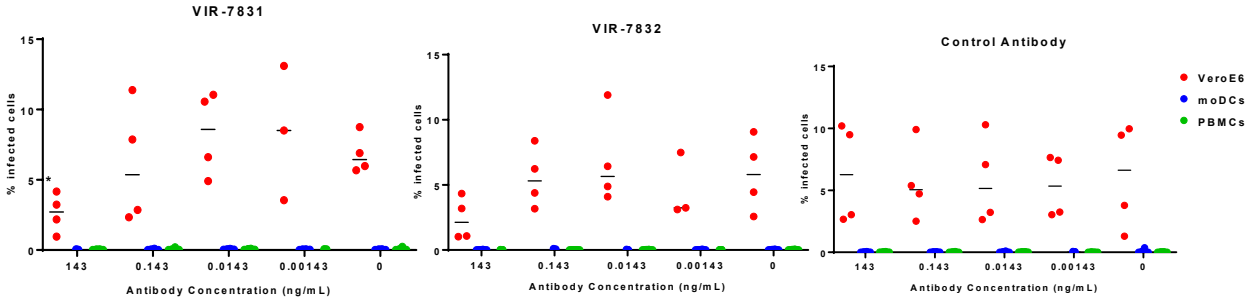

b)

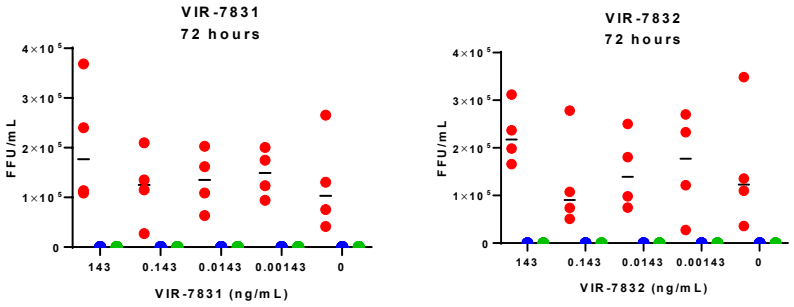

c)

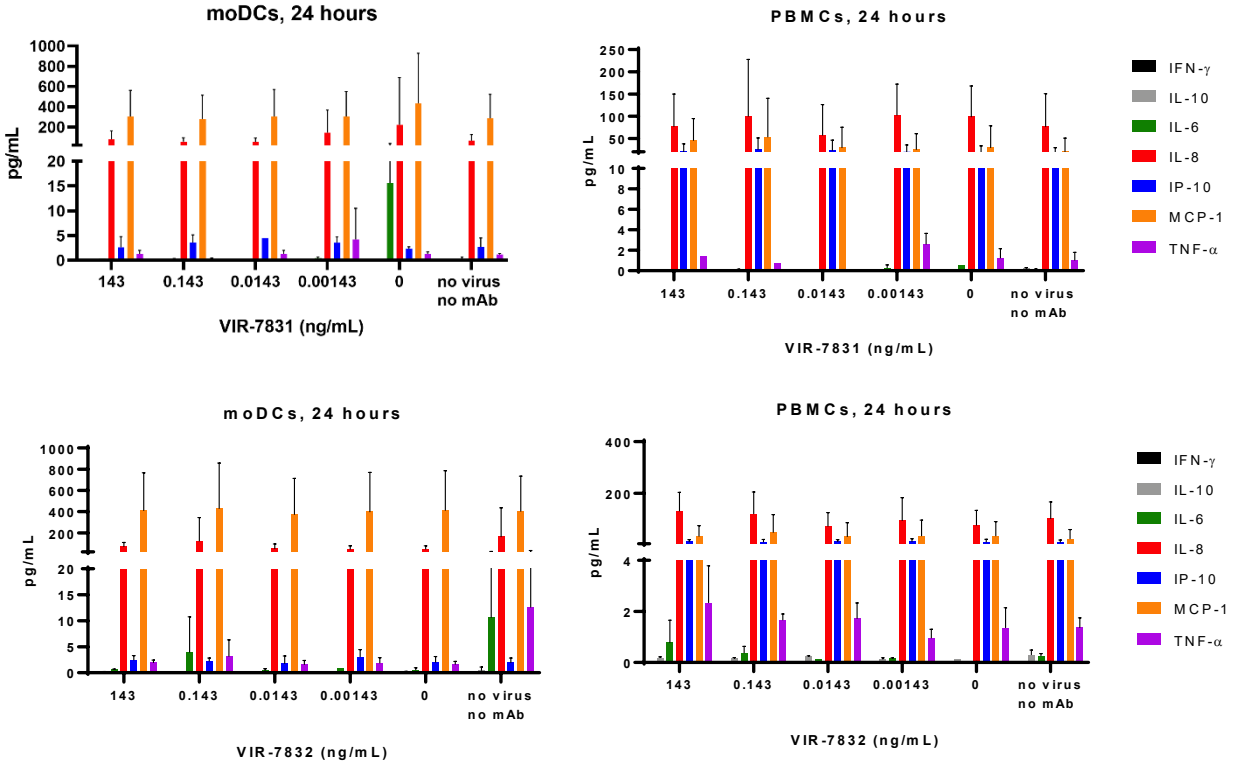

Supplemental Figure 3

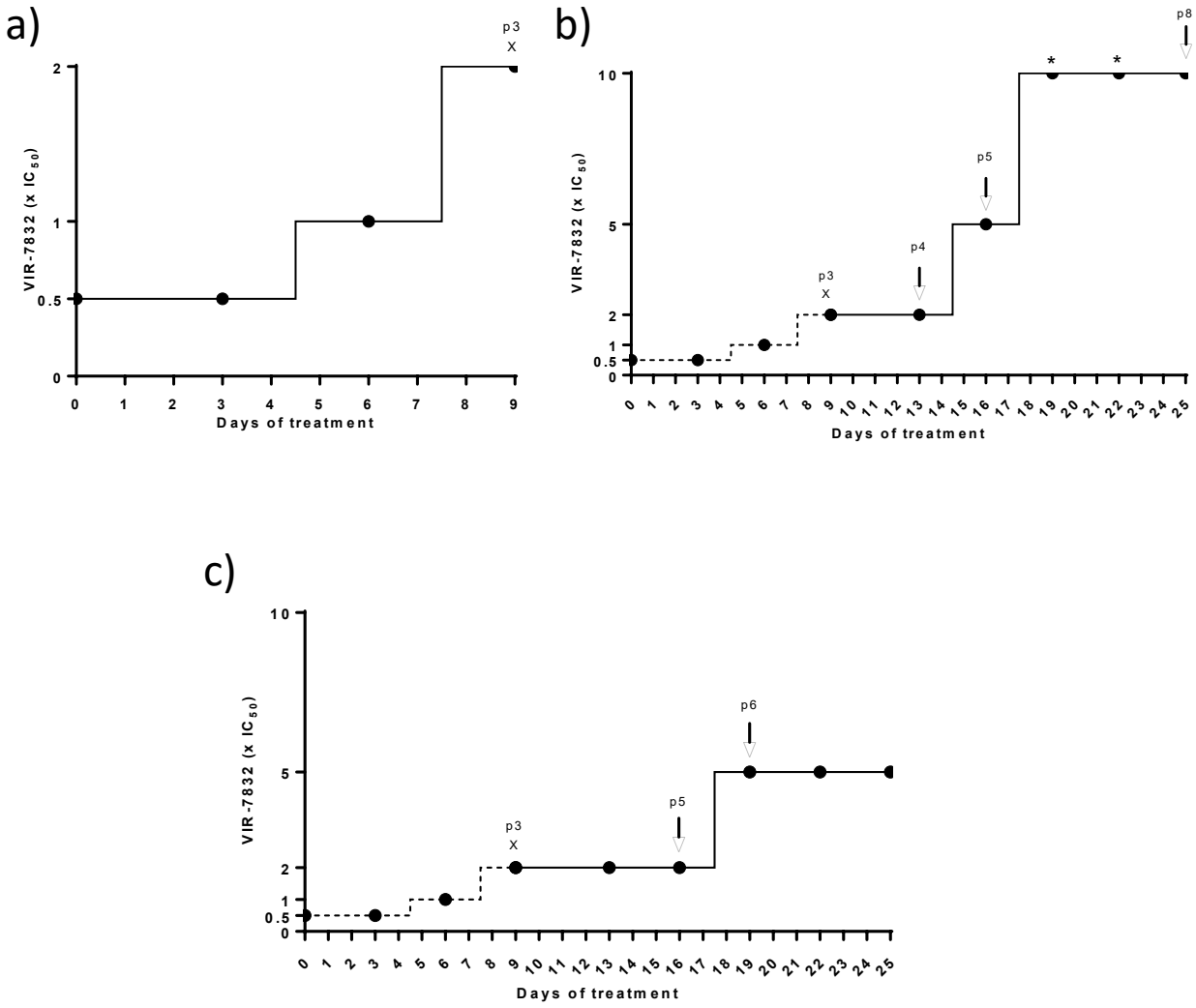

Supplemental Table 1

Passage	**Spike Gene Amino Acid Substitution (Freq)**[a,b]	**Fold Change in IC_{50} vs WT**[c]
SARS-CoV-2 virus stock[c]	H66R (5.7%) N74K (12.6%) T76I (5.6%) 215-216insKLRS (60.9%) H655Y (3.1%)	NA
VIR-7832 Lineage 1, passage 4	215-216insKLRS (74.5%) 675-679 del (20.6%)	5.64
VIR-7832 Lineage 1, passage 5	215-216insKLRS (74.6%) 675-679del (66.0%)	5.93
VIR-7832 Lineage 1, passage 8	215-216insKLRS (74.7%) E340A (98.7%) 675-679del (84.5%)	>10
VIR-7832 Lineage 2, passage 5	215-216insKLRS (73.9%) 675-679del (47.3%) R682W (4.9%) V1128F (3.5%)	5.40
VIR-7832 Lineage 2, passage 6	215-216insKLRS (75.3%) 675-679del (74.2%) R682W (4.9%) V1128F (30.9%)	6.54

Del: deletion; freq: frequency; ins: insertion; NA: not applicable; WT: wild type

[a] Spike gene sequences were compared to a SARS-CoV-2 reference sequence (NCBI: NC_045512.2) to call variants

[b] Sequence changes are reported for the SARS-CoV-2 input virus.

[c] Fold change IC50 values were compared to SARS-CoV-2 virus stock

Supplemental Table 2

Amino Acid Changes in Spike protein	VIR-7831		VIR-7832	
	Geomean Neutralization IC_{50} (ng/mL)	Fold Change Relative to Wild-Type	Geomean Neutralization IC_{50} (ng/mL)	Fold Change Relative to Wild-Type
Wild Type[a]	104.46	NA	100.75	NA
E340A	> 10,000	>100	> 10,000	> 107
R682W	53.96	0.52	47.78	0.49
V1128F	50.65	0.53	49.69	0.60